AD_____

GRANT NUMBER DAMD17-94-J-4041

TITLE: Cloning and Characterizing Genes Involved in Monoterpene Induced Mammary Tumor Regression

PRINCIPAL INVESTIGATOR: Michael N. Gould, Ph.D.
Eric A. Arizai, Ph.D.

CONTRACTING ORGANIZATION: University of Wisconsin
Madison, Wisconsin 53706

REPORT DATE: October 1996

TYPE OF REPORT: Annual

PREPARED FOR: Commander
U.S. Army Medical Research and Materiel Command
Fort Detrick, Frederick, Maryland 21702-5012

DISCLAIMER NOTICE

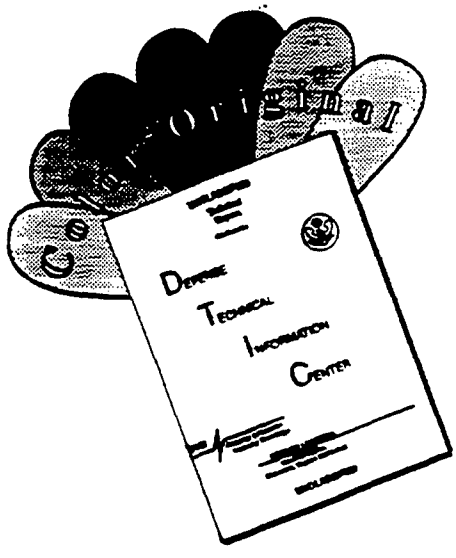

THIS DOCUMENT IS BEST QUALITY AVAILABLE. THE COPY FURNISHED TO DTIC CONTAINED A SIGNIFICANT NUMBER OF COLOR PAGES WHICH DO NOT REPRODUCE LEGIBLY ON BLACK AND WHITE MICROFICHE.

REPORT DOCUMENTATION PAGE

Form Approved
OMB No. 0704-0188

1. AGENCY USE ONLY *(Leave blank)*	2. REPORT DATE	3. REPORT TYPE AND DATES COVERED
	October 1996	Annual (1 Sep 95 - 31 Aug 96)

4. TITLE AND SUBTITLE
Cloning and Characterizing Genes Involved in Monoterpene Induced Mammary Tumor Regression

5. FUNDING NUMBERS
DAMD17-94-J-4041

6. AUTHOR(S)
Michael N. Gould, Ph.D.
Eric A. Arizai, Ph.D.

7. PERFORMING ORGANIZATION NAME(S) AND ADDRESS(ES)
University of Wisconsin
Madison, Wisconsin 53706

8. PERFORMING ORGANIZATION REPORT NUMBER

9. SPONSORING/MONITORING AGENCY NAME(S) AND ADDRESS(ES)
Commander
U.S. Army Medical Research and Materiel Command
Fort Detrick, MD 21702-5012

10. SPONSORING/MONITORING AGENCY REPORT NUMBER

11. SUPPLEMENTARY NOTES

12a. DISTRIBUTION / AVAILABILITY STATEMENT
Approved for public release; distribution unlimited

12b. DISTRIBUTION CODE

13. ABSTRACT *(Maximum 200*

Monoterpene-induced/repressed genes were identified in regressing rat mammary carcinomas treated with dietary limonene using a newly developed method termed subtractive display. The subtractive display screen identified 42 monoterpene-induced genes comprising 9 known genes and 33 unidentified genes, as well as 58 monoterpene-repressed genes comprising 1 known gene and 57 unidentified genes. Several of the identified differentially expressed genes are involved in the mitoinhibitory transforming growth factor β signal tranduction pathway, as demonstrated by isolation of the mannose 6-phosphate/insulin-like growth factor II receptor and the transforming growth factor β type II receptor. The monoterpene induced/repressed genes indicate that apoptosis and differentiation act in concert to effect carcinoma regression. Apoptosis is suggested by the cloning of a marker of programmed cell death, lipocortin 1. Consistent with a differentiation/remodeling process occurring during tumor regression, subtractive display identified YWK-II and neuroligin 1. Thus far, of the cDNAs putatively identified as differentially expressed in this complex *in situ* carcinoma model, 5 were tested, and each one has been confirmed to be differentially expressed. Additionally, many of the identified known genes are expressed as rare transcripts and exhibit small but significant changes in abundance.

14. SUBJECT TERMS	15. NUMBER OF PAGES
Breast Cancer Therapy, Breast Cancer Prevention, Monoterpene, Gene Cloning, Subtractive Hybridization, Rattus Norvegicus Breast Cancer	52
	16. PRICE CODE

17. SECURITY CLASSIFICATION OF REPORT	18. SECURITY CLASSIFICATION OF THIS PAGE	19. SECURITY CLASSIFICATION OF ABSTRACT	20. LIMITATION OF ABSTRACT
Unclassified	Unclassified	Unclassified	Unlimited

FOREWORD

Opinions, interpretations, conclusions and recommendations are those of the author and are not necessarily endorsed by the US Army.

___ Where copyrighted material is quoted, permission has been obtained to use such material.

V Where material from documents designated for limited distribution is quoted, permission has been obtained to use the material.

V Citations of commercial organizations and trade names in this report do not constitute an official Department of Army endorsement or approval of the products or services of these organizations.

V In conducting research using animals, the investigator(s) adhered to the "Guide for the Care and Use of Laboratory Animals," prepared by the Committee on Care and Use of Laboratory Animals of the Institute of Laboratory Resources, National Research Council (NIH Publication No. 86-23, Revised 1985).

___ For the protection of human subjects, the investigator(s) adhered to policies of applicable Federal Law 45 CFR 46.

V In conducting research utilizing recombinant DNA technology, the investigator(s) adhered to current guidelines promulgated by the National Institutes of Health.

V In the conduct of research utilizing recombinant DNA, the investigator(s) adhered to the NIH Guidelines for Research Involving Recombinant DNA Molecules.

V In the conduct of research involving hazardous organisms, the investigator(s) adhered to the CDC-NIH Guide for Biosafety in Microbiological and Biomedical Laboratories.

Eric V. Knatz 11/14/90

PI - Signature Date

Table of Contents

Annual Report for Grant Number DAMD17-94-J-4041

Title: Cloning and Characterization of Genes Involved in Monoterpene-Induced Mammary Tumor Regression

INTRODUCTION

The monoterpenes limonene and perillyl alcohol, an emerging class of naturally occurring anti-cancer compounds, are highly effective against a variety of rodent organ-specific cancer models (reviewed in 1, 2). Dietary administration of monoterpenes is effective for chemoprevention and chemotherapy of both 7,12-dimethylbenz[*a*]anthracene (DMBA)[1]-induced and *N*-methyl-*N*-nitrosourea (NMU)-induced rat mammary carcinomas (3-10). As a chemotherapeutic agent, dietary 10% limonene caused ~66% of advanced DMBA- or NMU-induced carcinomas to completely regress and an additional ~23% to partially regress (6). Moreover, a 2% perillyl alcohol diet resulted in 50% complete and an additional 25% partial regression of advanced DMBA-induced mammary carcinomas (7). Treatment with both monoterpenes at these anti-cancer doses did not cause systemic toxicity. Monoterpenes are currently being tested in Phase I clinical trials on advanced cancer patients in England (11) and the United States[2].

Several observations suggest that monoterpene-mediated mammary carcinoma regression may involve a differentiation/remodeling process. Histopathology of monoterpene-treated, actively regressing tumors displays regions of dense anaplastic epithelium characteristic of mammary carcinomas and regions of a remodeled epithelial compartment. Regressing carcinomas do not show increased levels of lymphocyte infiltration, inflammation, or necrosis (6). Furthermore, monoterpene-treatment of neuro2A neuroblastoma cells causes morphologic differentiation within 4 hours as characterized by neurite outgrowths (12).

Monoterpenes inhibit enzymes in the mevalonate-lipid metabolism pathway, including a selective inhibition of isoprenylation of 21-26 kDa small G proteins (13-15) and inhibition of ubiquinone (CoQ) and cholesterol synthesis (16). Inhibition of isoprenylation may affect signal transduction pathways because unprocessed or non-prenylated small G proteins are not properly localized within the cell and are thus non-functional (17). Furthermore, investigations into gene expression and protein level alterations associated with monoterpene-mediated tumor regression revealed a large increase of the mitoinhibitory transforming growth factor β1 (TGFβ1) and the mannose 6-phospate/insulin-like growth factor II receptor (M6P/IGF2R), which both facilitates latent-TGFβ1 activation and degrades the mammary mitogen insulin-like growth factor II (IGF2; 18). Interestingly, while M6P/IGF2R RNA expression was significantly induced 2-fold in 10% limonene-treated carcinomas, the induced RNA expression of M6P/IGF2R was not observed in the non-responsive 10% limonene-treated carcinomas (19).

We hypothesized that biochemical events in the cytoplasm modify signal transduction leading to altered gene expression. Thus, in order to further elucidate the monoterpenes' mechanism of cancer chemoprevention and chemotherapy, we screened for differentially expressed genes in 10% limonene-treated, DMBA-induced, advanced mammary carcinomas resected at mid-regression.

Complex tissues, such as mammary carcinomas, are composed of large heterogeneous cell populations and hence require sensitive gene expression screening methods. This is because a particular gene may be induced or repressed only in a specific cell type, which would be diluted by all the other cell types. In order to achieve the required level of sensitivity, the subtraction method of Wang and Brown (20) was initially chosen because this approach uses polymerase chain reaction (PCR) amplification to generate a renewable source of cDNA for multiple rounds of subtraction, and the method efficiently removes commonly expressed cDNA from the experimental and control cDNA pools to allow for enrichment of differentially expressed genes. However, cloning the differentially expressed cDNAs involves cycles of classical probe hybridization experiments to isolate only a few clones at a time, followed by subtraction of the newly cloned cDNAs from the library. The cloning cycle is repeated until the library is completely screened, which may take 20-30 or more cloning cycles and thus renders this methodology inefficient.

A possible alternative method considered was Liang and Pardee's differential display (21), since it is also a PCR-based technique that selectively amplifies subsets of cDNAs based on primer design applied to two matched but non-subtracted cDNA populations. This technique clones genes quickly but only ~10% of the genes are differentially expressed when tested (22-24). Problems with reproducibility are probably due to the low stringency in annealing of primers, though recent modifications in primer design and experimental protocol have somewhat improved reproducibility (25-28). In addition, because the primers effectively anneal as 6- or 7-base oligomers of arbitrary sequence, a statistical argument is needed to determine when the libraries are sufficiently screened (21). Furthermore, there exists a high level of background noise in differential display due to the vast majority of competing heterologous RNA. Differential display shows a strong bias toward identifying abundant mRNAs (29). An efficient gene expression screen should identify rare transcripts, which account for ~90% of mRNA species in most cells (29).

In order to more efficiently identify differentially expressed monoterpene target genes, we developed and characterized an alternative approach, termed subtractive display (SD), which incorporates the strengths and minimizes the weaknesses of subtractive hybridization and differential display. We have applied SD to identify differentially expressed genes in limonene-treated advanced rat mammary carcinomas.

Experimental Procedures

Summary of Subtractive Display (SD) Methodology- A flowchart of the SD methodology is given in Fig. 1. cDNA was generated from two matched tissue sources, or for this set of experiments, monoterpene-treated, regressing, mammary carcinomas (+cDNA) and control, non-treated carcinomas (-cDNA). +/- cDNA was fragmented with restriction endonucleases followed by ligation of symmetrical linkers. The sequence at the cDNA fragment ends reflects the methods used to generate the cDNA libraries and restriction endonuclease recognition sites, and hence, are non-random sequences. The subtractive process involves multiple rounds of hybridization and PCR amplification, which renews the cDNA source. +cDNA was subtracted from -cDNA, and concurrently, -cDNA was subtracted from +cDNA, to derive induced and repressed genes, respectively. Subtracted cDNA was subcloned into a trimming plasmid and subjected to three cycles of precise, unidirectional deletions. The trimming procedure serves to reconfigure the subtracted libraries such that one end of the cDNA is composed of randomized sequence and both ends of the cDNA fragment are flanked by different or asymmetric primers. The subtracted, reconfigured cDNA libraries were PCR-displayed using 16 sets of primers consisting of 1 fixed primer and 1 of 16 subpopulation primers. The subpopulation primers are designed to anneal with a 2-base overlap (3' end of primer) of the randomized sequence end of the reconfigured cDNA. The penultimate 2-bases of the 3' end of the subpopulation primers were a specific combination of 1 of 16 (2^4) possible 2-base combinations, thus selecting for PCR-amplification of a subpopulation of subtracted, reconfigured cDNA. Individual cDNA bands were isolated and characterized to confirm differenential expression.

Preparation of cDNA from Mammary Carcinomas- Regressing (monoterpene-treated) and non-regressing (control, not treated) carcinomas for all studies were generated by the following protocol. Virgin female Wistar-Furth inbred rats at 50-55 days of age were given a single dose of DMBA (50 mg/kg body weight) by gastric intubation. Developing carcinomas were followed by palpation until they grew to $\geq$ 10 mm in diameter, at which time rats were randomized to either a monoterpene diet of 10% (w/w) *d*-limonene or a control diet and pair-fed. Carcinomas from rats on monoterpene diet that regressed to 50% of their maximum diameter were resected. All remaining carcinomas were collected by 15 weeks after diet randomization. All animal use was in compliance with NIH guidelines for humane care and was approved by the University of Wisconsin-Madison Medical Center Animal Use Committee.

Total tumor RNA was isolated using RNAzol B Reagent (Tel-Test, Friendswood, Texas, USA) and poly(A)+ RNA was isolated using the PolyATtract System 1000 (Promega, Madison, WI, USA) following the manufacturer's directions. The Superscript Plasmid System (Gibco BRL Life Technologies, Gaithersburg, MD, USA) was used for double-stranded cDNA synthesis from poly(A)+ RNA. 5 µg of cDNA synthesized from 7 regressing and 7 non-regressing carcinomas were pooled and termed +cDNA and -cDNA, respectively. A portion of the +cDNA and -cDNA

was reserved for construction of non-fragmented cDNA plasmid libraries with the vector pSport1 and transformed by electroporation into Electromax Efficiency DH12S *E. coli* host cells (Gibco BRL Life Technologies).

Subtraction- We used the PCR-based subtractive hybridization method of Wang and Brown described in detail elsewhere (20). In brief, the subtraction protocol operates by fragmenting the cDNA with restriction endonucleases (i. e. *Alu*I and *Alu*I plus *Rsa*I) and ligating onto their termini 21 bp oligodeoxynucleotide linkers having a 5' blunt end and a 4-base 3' overhang. The flush end contained an *Eco*RI site. Following linker ligation, the fragmented cDNAs are subjected to PCR amplification using the 21-bp linkers as primers (sequences given in 20). It is assumed that cDNA fragments common to both +cDNA and -cDNA populations were amplified equally, while different cDNA fragments within a population may be differentially amplified. Dependent on the direction of subtraction, whether up- or down-regulated cDNAs were being enriched, either +cDNA or -cDNA and their derived populations were tracer or driver cDNA. Thus in the following, driver or tracer cDNA is specified but not if +cDNA or -cDNA was used. 50 μg of driver cDNA was completely digested with *Eco*RI to suppress contaminating driver cDNA from being amplified. Driver cDNA was then photobiotinylated and combined with 2.5 μg non-biotinylated tracer cDNA. The mixture was completely denatured by boiling and then cooled for a long hybridization (20 hours). Addition of streptavidin led to formation of streptavidin-biotin-DNA complexes that were removed by several phenol-chloroform extractions. Subtracted tracer cDNA (termed 1cDNA) was again subtracted from 25 μg biotinylated driver cDNA, this time for a short hybridization of 2 hours to yield 2cDNA. +2cDNA and -2cDNA were PCR amplified. 2.5 μg non-biotinylated tracer 2cDNA was subtracted against 50 μg *Eco*RI treated-biotinylated driver 2cDNA for a long hybridization followed by 25 μg driver 1cDNA for a short hybridization, resulting in 4cDNA, which was then PCR amplified. Another similar cycle was performed giving 6cDNA.

The subtractive hybridization process was monitored by displaying the cDNA libraries after each round of subtraction on a sequencing gel. The cDNA libraries were amplified using a primer derived from the original linker sequence ligated onto the cDNA fragment ends but modified by deletion of the two 5' bases and the addition of the 2 mixed bases A/T and G/C on the 3' end that overlaps the cDNA insert [5'-CTTGCTTGAATTCGGACTA(A/T)(C/G)-3'], giving 4 possible primers and 16 possible primer pairs. This mixed primer anneals at both ends of the cDNA fragments and because of the two mixed bases at the 3' end that overlap the cDNA insert, the sequence selectively amplifies a representative cDNA subpopulation such that individual bands are visualized (Fig. 2). The PCR temperature profile used was 94° C - 5 min hot start followed by 94° C - 1 min, 50° C - 1 min, 72° C - 2 min for 30 cycles. The PCR products were resolved on a 5% polyacrylamide gel and visualized by exposure to X-OMAT AR film (Kodak, Rochester, New York, USA).

Trimming Cycles- The subtracted cDNA libraries were next reconfigured such that unique primer sites flank the cDNA insert. This was accomplished by cloning the libraries into the

trimming plasmid pTRIM14 using the *Eco*RI site within the libraries' linkers and the *Eco*RI site located 2 bp downstream of pTRIM14's trimming cassette (30). This procedure resulted in deletion of 9 bp of the cDNA libraries' linker ends, allowing 12 bp to remain. Precise unidirectional deletions were then generated on one end of the subtracted cDNA libraries by three trimming cycles of 14 bp each. We followed the trimming cycle protocol as detailed elsewhere (30). In brief, pTRIM14's trimming cassette contains *Bse*RI and *Bsg*I recognition sites configured such that stepwise digestion first with *Bsg*I and then *Bse*RI produces cleavage of DNA 16/14 nt distal and 4/2 nt proximal, respectively, relative to the 3' end of the cassette, thus conserving the trimming cassette but cutting into the 5' end of the cDNA fragment. The trimming cycle continues by treatment with Mung Bean nuclease to remove single-stranded ends of the linearized DNA and finally re-circularization of the plasmids with T4 DNA ligase. Noteworthy, cDNA fragments that may contain *Bsg*I or *Bse*RI are not lost from the library since a portion of the cDNA fragment is retained. Additionally, this trimming procedure was shown to produce deletions with very high efficiency on a population of plasmids (30).

PCR- All PCR reactions were carried out using the following conditions unless otherwise stated. In a final reaction volume of 50 µl, PCR was performed using 200 µM of each dNTP, 400 nM of each primer, and 2.5 units of AmpliTaq DNA polymerase (Perkin Elmer, Foster City, CA, USA). The 1X PCR buffer was composed of 50 mM KCl, 10 mM Tris-HCl (pH 8.3), 1.5 mM $MgCl_2$, and 0.001% (w/v) gelatin. All primers were synthesized at the Wisconsin Biotechnology Center (Madison, WI, USA) unless otherwise stated.

Subtractive Display (SD)- The subtracted and reconfigured cDNA libraries were displayed using sets of a fixed primer (5'-ATTACGAATTCGGACTA-3') and 1 of 16 possible subpopulation primers (5'-GAGGAGGTGCAGTANN-3'), as determined by the specific combination of the two variable penultimate 3' bases designated by NN (Fig. 1 and 3). An explanation of these primer sequences is given under Results. The nucleotide concentration for PCR used was 20 µM of each dNTP plus 10 µCi of [α-^{35}S] dATP, and the PCR temperature profile used was 94° C - 5 min hot start followed with 94° C - 1 min, 59° C - 1 min, 72° C - 1 min for 30 cycles and lastly 72° C - 10 min to ensure double stranded cDNA. Labelled PCR products were resolved on a 5% polyacrylamide sequencing gel and visualized by a PhosphorImager (Molecular Dynamics, Sunnyvale, CA, USA). These experiments were also performed in parallel by omitting the radiolabel and instead silver staining the gel (31) to visualize the bands directly, which greatly improves efficiency of band isolation. Unique bands were excised, eluted from the gel and reamplified using the same fixed PCR primer and a modified subpopulation primer, or pan primer, that amplifies the entire cDNA population. The pan primer has two C bases and an *Eco*RI site (underlined) added to the 5' end and the two terminal variable 3' bases removed from the subpopulation primer (5'-CCGAATTCGAGGAGGTGCAGTA-3). Isolated cDNA fragments were digested with *Eco*RI, subcloned into the multiple cloning site of the pSport1 plasmid (Gibco BRL Life Technologies), and transformed by electroporation into Electromax Efficiency DH12S *E. coli* host cells (Gibco BRL Life Technologies).

Sequence Analysis- All subcloned cDNA fragments were sequenced using the M13/pUC forward primer and the PRISM Ready Reaction Dye Deoxy Terminator Cycle Sequencing Kit (Perkin Elmer), following the manufacturer's protocol. The sequencing reaction products were resolved on an ABI PRISM Automated DNA Sequencer (Advanced Biotechnologies Inc., Columbia, MD, USA). The monoterpene-induced gene (MIG) and monoterpene-repressed gene (MRG) sequences were compared to a non-redundant nucleotide sequence database that includes sequences from the Brookhaven Protein Data Bank, Genbank, Genbank updates, EMBL and EMBL updates using the BLAST algorithm at the National Center for Biotechnology Information (NCBI) (32).

Competitive Reverse Transcriptase-PCR (RT-PCR)- Relative RNA expression levels between regressing (10% limonene-treated) and non-regressing (control, not treated) mammary carcinomas were determined by competitive RT-PCR (33-38). The competitive RT-PCR assay involved PCR of a target gene (*i. e.*, a MIG/MRG cDNA,) competing for amplification with its exogenously added MIMIC, and amplification of an internal standard [*i.e.*, glyceraldehyde 3-phosphate dehydrogenase (G3PDH)] competing for amplification with its exogenously added MIMIC, for a total of 4 PCR products per sample. A MIMIC is a piece of heterologous DNA with flanking sequences identical to the primer sequences used for the target gene, such that a known amount of MIMIC is exogenously added for to enable simultaneous co-amplification with a target gene. In essence, the competitive RT-PCR assay normalizes the MIG/MRG cDNA to an external control (MIG/MRG MIMIC) and to an internal G3PDH control, which itself was normalized to an external control (G3PDH MIMIC). After the target MIG/MRG expression for each sample was normalized, its expression level in each sample of the control and regressing carcinoma groups was averaged and compared in order to determine fold-induction or fold-repression. Statistical significance was calculated using the two-tailed Student's *t* test.

Relative RNA expression levels for lipocortin 1 (LC1), transforming growth factor β type II receptor (TGFβIIR), and neuroligin 1 were determined by competitive RT-PCR. RNA was prepared from 5 individual regressing (10% limonene-treated) and 5 individual non-regressing (control, not treated) mammary carcinomas as described above. cDNA was generated using the 1st-Strand cDNA Synthesis Kit (Clontech Laboratories, Palo Alto, CA, USA). Primers were designed using Oligo 5.0 Primer Analysis software (National Biosciences, Plymouth, MN, USA), with the exception of the G3PDH primers (Clontech Laboratories). MIMICs were generated using the PCR MIMIC Construction kit (Clontech Laboratories). Generation of MIMICs involves a 1° PCR reaction using a composite primer, consisting of target gene or gene-specific primer sequence at the 5' end and heterologous DNA primer sequence on the 3' end. Next, an aliquot of the 1° PCR reaction was used as template in a 2° PCR reaction using only target gene or gene-specific primers. Primers and dNTPs were removed by passing the 2° PCR reaction over a Chromaspin-100 column (Clontech Laboratories) and the MIMIC was quantified by spectrophotometric analysis. Primer sequences and product sizes are given in Table 1. In a reaction volume of 50 µl, the final concentration of exogenously added PCR MIMICs were 4.0×10^{-2} amol/µl of LC1

MIMIC, 8.0 x 10^{-5} amol/µl of TGFβIIR MIMIC, 4.0 x 10^{-6} amol/µl of neuroligin 1 MIMIC, and 4.0 x 10^{-5} amol/µl G3PDH MIMIC 1 or G3PDH MIMIC 2. The PCR temperature profile used for all competitive RT-PCR experiments was 94° C - 5 min hot start followed by 94° C - 1 min, 60° C - 1 min, 72° C - 2 min for 30 cycles, with the exception of LC1, which required an annealing temperature of 58° C. PCR products were resolved on a 2% NuSieve GTG agarose gel (FMC BioProducts, Rockland, ME, USA). Primers were 5' end-labelled with fluorescein during their synthesis, thereby allowing PCR product quantitation using a FluorImager (Molecular Dynamics).

Results

An overview of the SD methodology is presented in Fig. 1. An evaluation of each aspect of this technology is presented below.

Subtraction of cDNA Libraries- The subtractive hybridization procedure developed by Wang and Brown (20) served to remove commonly expressed cDNA fragments and enrich for those that are differentially expressed. The subtraction process involved initial fragmentation of the cDNA libraries with restriction endonucleases and ligation of 21 bp oligodeoxynucleotide linkers onto the cDNA fragment ends, thus allowing for a renewable source of cDNA by PCR. The monoterpene-treated derived cDNA (+cDNA) was subtracted against control, non-treated derived cDNA (-cDNA) to enrich for monoterpene-induced genes (MIG). The inverse subtraction, control, non-treated cDNA subtracted against monoterpene-treated cDNA, was also performed to enrich for monoterpene-repressed genes (MRG). The cDNA libraries were subjected to cycles of alternating long (20 hrs) and short (2 hrs) hybridizations for a total of 6 hybridizations. We monitored the subtractive process by PCR amplification of the cDNA libraries after each round of subtraction, before the libraries were reconfigured using pTRIM14, and displayed them on a sequencing gel. A representative cDNA subpopulation was PCR amplified by modifying the 21 bp primer, which anneals to the linkers initially ligated onto the fragment ends, such that the two 5' bases were removed and two mixed bases were added to the 3' end, thus overlaping the cDNA insert, as described in detail under Experimental Procedures. Fig. 2 demonstrates the efficiency of the subtractions. The unsubtracted +cDNA and -cDNA lanes showed smears, while with each additional cycle of subtraction, individual bands became increasingly prominent. Furthermore, the banding patterns between the subtracted +cDNA and the subtracted -cDNA lanes were reproducible, indicating that specific cDNA fragments were increasingly enriched while others were driven out of the population. Efficiency of subtraction was further tested by isolating 2 prominent bands from both the +6cDNA and -6cDNA lanes, followed by subcloning and sequencing the cDNAs by similar methods of clone characterization discussed below. One of the derived +6cDNA fragments was identified by a nucleotide database search using the BLAST algorithm (32) as the YWK-II gene, which was again identified at the end of the SD process (indicated by an arrow; compare Fig. 2 and 5) and shown to be differentially expressed as discussed below.

Reconfiguration and Display of the Subtracted Libraries- The subtracted cDNA libraries were next reconfigured for the display step. The libraries were reconfigured because during their construction both ends of the cDNA fragments were ligated to the same linker, *i. e.* the ends are symmetrical. Symmetrical primer sites limits the ability to display the subtracted cDNA libraries because a primer designed to overlap the cDNA insert by 2-bases will anneal on both ends of the cDNA fragment, thus not permitting all 2-base independent combinations at both cDNA insert ends for complete screening of the libraries. In addition, the first few bases at both ends of the cDNA fragments in the subtracted libraries are not random but reflect both the methods used to make the

cDNA (priming the poly(A) tail with a sequence containing a *Not*I site) and that used to fragment the cDNA (restriction digestion with two 4-base cutters). One end of each cDNA fragment needs to be random sequence, such that a subpopulation primer will selectively amplify a small number of distinct bands during the subtractive display step, as discussed below. Reconfiguration of the subtracted cDNA libraries was accomplished by cloning the subtracted libraries into pTRIM14 (30) and processing the cDNA libraries through 3 cycles of precise, unidirectional, 14 bp trimming, as discussed under Experimental Procedures. pTRIM14 was constructed with a trimming cassette composed of *Bsg*I and *Bse*RI recognition sites. A trimming cycle operates by sequential digestion with *Bsg*I and then *Bse*RI to produce cuts 16/14 nt distal and 4/2 nt proximal, respectively, relative to the 3' end of the trimming cassette, thereby producing a deletion onto the 5' end of the cDNA fragment but retaining the trimming cassette. Single-stranded DNA ends are removed by digestion with Mung Bean nuclease followed by ligation with T4 DNA ligase. The subtracted cDNA libraries were subjected to three trimming cycles, generating +6Δ3 and -6Δ3 cDNA (6 rounds of subtraction and 3 cycles of trimming). Accounting for subcloning the subtracted libraries into pTRIM14 (deletion of 9 bp) and 3 trimming cycles, the entire 21 bp linker plus an additional 30 bp on the left end of the cDNA libraries was completely removed, leaving one cDNA end with randomized sequence, as described in greater detail under Experimental Procedures.

The reconfigured, subtracted cDNA libraries were displayed by consecutive amplification of cDNA subpopulations using 16 sets of PCR primers (Fig. 3 and 5). In each primer set, one primer is always the same or fixed and anneals at the unmodified or right (3') end of the cDNA fragment. This fixed primer is a 17-mer with a sequence of 5'-ATTACGAATTCGGACTA-3', and comprised in the 5'-3' direction of pTRIM14 sequence, an *Eco*RI site (underlined), and original linker sequence. The second primer in each primer set anneals on the randomized or left (5') end of the cDNA fragment and is termed the subpopulation primer. The 5' end of the subpopulation primer anneals to 14 bp of pTRIM14 sequence, and its 3' end overlaps the cDNA fragment by 2 bp. These two 3' bases in each individual subpopulation primer will consist of 1 of the 16 possible 2-base combinations, resulting in a subpopulation primer sequence of 5'-GAGGAGGTGCAGTANN-3' (Fig. 2). Therefore, 1 of a total of 16 sets of PCR primers results in selective annealing and amplification of a subpopulation of the cDNA, and consecutive amplification with each of the sixteen sets of primers allows complete screening of the libraries.

In order to maximize subpopulation selective amplification and minimize redundancy of clone isolation, the dNTP concentration and annealing temperature of the SD reactions were optimized. Optimization of dNTP concentration and annealing temperature increases the number of unique bands in one subpopulation and reduces the number of bands that appear multiple times across various subpopulations due to mispriming of the two terminal 3' bases of the subpopulation primer. Initial SD optimization experiments used representative sets of SD primers including the fixed primer and the subpopulation primers CC, AC, AG, and GA, as specified by the variable bases of the subpopulation primer (or the two 3' penultimate bases of the sequence 5'-GAGGAGGTGCAGTANN-3'), at dNTP concentrations of 200 μM, 20 μM, 10 μM and 2 μM,

all at an annealing temperature of 59° C (data not shown). The 20 μM SD reaction amplified the cDNA fragments efficiently with moderate band redundancy, while the 10 μM SD reaction amplified the cDNA fragments with lower efficiency but less band redundancy. SD conditions were further refined using the subpopulation primer sets AC, AG, and GA because of their similar sequence. These three primer sets were used in SD experiments under annealing conditions of 57° C, 59° C, 61° C, and 63° C using 10 μM and 20 μM dNTP (Fig. 3). SD reaction conditions of 20 μM dNTP and an annealing temperature of 59° resulted in reproducible efficient amplification with relatively low redundancy of bands.

SD reactions were performed with all 16 sets of subpopulation primers using both 10 μM dNTP (data not shown) and 20 μM dNTP (Fig. 5). Both experiments were performed in parallel, with radiolabel and without radiolabel in order to isolate bands by silver staining (31). Unique bands from the SD experiment using 20 μM dNTP were excised, eluted from the gel, reamplified using the same fixed PCR primer and a pan primer that amplifies all cDNA fragments (sequence given under Experimental Procedures), and PCR products were subcloned into pSport1. Individual subcloned cDNAs were designated as a monoterpene-induced gene (MIG) or monoterpene-repressed gene (MRG) by virtue of the cloning process (*i.e.*, whether the cDNA originated from the monoterpene-treated +cDNA or the untreated control -cDNA, respectively).

Characterization of Differentially Expressed Clones- We isolated 42 MIG and 58 MRG rat cDNAs (Table 2), all of which were sequenced and compared against sequence databases using the BLAST algorithm for possible identification. A MIG/MRG clone was defined to be a known gene if it shows ≥ 95% sequence identity over the entire cDNA fragment with a known gene from the sequence data base. The cDNA insert sizes ranged from 45 to 312 bp due to the methods used for library generation, modification, and cloning. Considering the MIG cDNAs as one group, 9 were known, of which 3 were identified by more than 1 MIG cDNA. Additionally, 33 MIG cDNAs were not identified in the sequence database. Considering the MRG cDNAs as one group, 1 was a known gene and 57 MRG cDNAs were not identified in the sequence database. The identification of genes was limited due to our strict criteria for sequence identity plus the fact that our sequences were from rat whose representation in the databases is limited.

More than 1 cDNA fragment, varying in molecular weight, identified cytochrome c oxidase subunit II (COX II), sperm membrane protein YWK-II (39), and Y89 (5' end similar to YWK-II) (Table 2). The multiple cDNA fragments that identified each of these genes had common sequences but differed in the size of the cDNA fragment; for example, of the 6 cDNAs that identified COX II, all the clones shared 70 bp while the largest clone (MIG-27) had an additional 32 bp not found in the smallest clone (MIG-3).

The potential of the SD screen to identify differentially expressed genes was suggested by the isolation of M6P/IGF2R as MIG-42. We have previously shown that the M6P/IGF2R was induced 2.0-fold ($P \leq 0.002$) at the RNA level in 10% limonene-treated, regressing mammary carcinomas using an RNase Protection Assay (RPA) (Table 3; 19).

We next tested the differential expression of other identified MIG/MRG clones. We initially confirmed that YWK-II, a gene identified by 7 separate MIG clones (Table 2), was induced 2.9-fold ($P \leq 0.00006$) in a panel of 10% limonene-treated regressing carcinomas relative to control non-regressing carcinomas (Table 3). Expression was quantitated by Northern blot analysis and a PhosphorImager (Molecular Dynamics). YWK-II was also found to be most highly expressed in rat brain, moderately expressed in normal mammary gland, liver, and kidney, and at low levels in the spleen (data not shown).

However, Northerns and RPAs use ~1 μg of polyA+ RNA or 10 μg of total RNA per sample. In order to conserve regressing tumor RNA, which is quite limited, we used competitive RT-PCR (48-53) to determine relative fold-induction or fold-repression of the remaining MIG/MRG cDNAs.

We tested the differential expression of MIG-12, identified as lipocortin 1 (LC1; 40), using the competitive RT-PCR assay described under Experimental Procedures (Fig. 6A). LC1 was induced 2.9-fold ($P \leq 0.00003$) in 10% limonene-treated regressing carcinomas relative to control non-regressing carcinomas (Fig. 6B, Table 3). We then examined LC1 RNA expression in the normal rat mammary gland by the same assay and found that LC1 was induced 3.1-fold ($P < 0.0005$) in the involuting mammary gland relative to the virgin mammary gland (data not shown). LC1 has been shown to be a marker for apoptosis in the involuting rat mammary gland (40).

The transforming growth factor β type II receptor (TGFβIIR; 41-44) was identified by MIG-33 and was induced 3.1-fold ($P < 0.0002$) in 10% limonene-treated regressing carcinomas relative to control non-regressing carcinomas (Table 3) by the competitive RT-PCR assay.

The SD screen identified neuroligin 1 as the clone MRG-31 (45). The competitive RT-PCR assay demonstrated neuroligin 1 expression to be repressed 8.8-fold in 1/5 or not detectable in 4/5 10% limonene-treated regressing carcinomas as compared to control carcinomas (Table 3).

CONCLUSIONS

The Subtractive Display Gene Expression Screen- In order to better understand the mechanism by which monoterpenes mediate tumor regression, we sought to identify differential gene expression patterns of actively regressing, advanced DMBA-induced rat mammary carcinomas treated with limonene relative to control (not treated) carcinomas. Due to the complexity of regressing tumor tissue, we required a very sensitive gene expression screening method that could detect relatively small alterations in gene expression levels and/or genes which may be expressed in low abundance. Because of these concerns, we integrated the strengths of subtractive hybridization and differential display into a new methodology termed subtractive display (SD).

Wang and Brown's subtractive hybridization method (20) generates cDNA for subtraction using PCR; however, clones are isolated by classical probe-hybridization techniques that require an undefined number of probing cycles. In contrast, SD cloning of enriched cDNAs is PCR-based and is therefore faster, more efficient and more sensitive. Unlike Liang and Pardee's differential display (21) where the 5' primer preferentially anneals somewhere upstream on the cDNA at a low temperature, the SD method uses a 16-base subpopulation primer and a 17-base fixed primer, each annealing at defined left and right linkers, respectively, on the cDNA fragment ends. In addition, annealing is performed at the highest temperature that still permits PCR to proceed (59° C). The combination of larger primers annealing at defined sites and a very high annealing temperature both contribute to high specificity and stringency, leading to high reproducibility between identical reactions. In addition, by primer design, the libraries are completely screened in 16 sets of reactions. Furthermore, because the cDNA libraries are subtracted before the display step, background noise is significantly reduced, thereby increasing reproducibility and detection of rare cDNAs. Moreover, there exists a potential for noise with differential display because differential display depends on precise registry of cDNA fragments in paired lanes such that unique bands are isolated; yet identical cDNA fragments in treated and non-treated populations may both be amplified but differ in size by a few base pairs. Alternatively, with SD, since all cDNA fragments are putatively differentially expressed because of the subtraction step, the precise registry of cDNA fragments in paired gel lanes is not necessary to identify the differentially expressed genes.

The SD screen identified the M6P/IGF2R, which was already known to be induced 2-fold at an RNA level in the epithelium of regressing carcinomas (19). This initially suggested that SD had high sensitivity. Additionally, every MIG/MRG clone tested for differential gene epression exhibited consistent differential expression across a panel of regressing carcinomas relative to non-regressing carcinomas, thus demonstrating the ability of SD to identify a high percentage of true differentially expressed clones. It should be noted that identification of a single gene by multiple clones versus one clone does not indicate the degree of differential expression; YWK-II was identified by 7 separate bands varying in molecular weight but showed a degree of induction similar to M6P/IGF2R, TGFβIIR, and LC1, all of which were identified by one clone (Table 2).

However, YWK-II may be more abundantly expressed. The multiple isolation of cDNA fragments that identify the same gene may have resulted from restriction digestion of the original cDNA before subtraction with *Alu*I and *Alu*I plus *Rsa*I, and/or cloning artifacts. Furthermore, band intensity does not indicate degree of differential expression, as there was no discernible difference in band intensity which identified neuroligin 1 and bands that identified the other known clones.

The Process of Monoterpene-Mediated Mammary Carcinoma Regression- Based upon histopathological analysis of monoterpene-treated regressing mammary carcinomas, the phenomenon of tumor regression was postulated to involve a differentiation/remodeling process (6). The identified MIG/MRG cDNAs are consistent with such a mechanism of regression. The present study is consistent with the hypothesized involvement of the TGFβ signalling pathway with tumor regression. The M6P/IGF2R and the TGFβIIR were identified as upregulated. The M6P/IGF2R facilitates latent-TGFβ1 activation (18, 46) and trafficks IGF2, a potent mammary carcinoma mitogen, into lysosomes for degradation (reviewed in 47). Also the M6P/IGF2R has been reported to be a tumor suppressor gene in both liver and breast cancer (48, 49). Interestingly, the SD screen identified the TGFβIIR, since it is postulated that breast tumors may not respond to TGFβ because the tumors express low levels TGFβ II receptors (50, reviewed in 51).

The SD screen isolated LC1, which is a marker for apoptosis during mammary gland involution. At the protein level, LC1 was induced 10-fold only in the alveolar epithelium, but remained at basal levels in ductal epithelium and stroma during involution, as determined by immunohistochemistry (40). Because RNA expression of LC1 in the context of the entire involuting mammary gland was not reported, we determined LC1 RNA expression during involution relative to the virgin mammary gland and found LC1 was induced 3.1-fold.

It should be noted that most overexpression of genes thus far analyzed was in the 2- to 3-fold range. In some cases this could be an underestimate due to the fact that our analysis methods averaged gene expression over cell types in a very heterogenous tissue. For example, LC1 was 3.1-fold overexpressed in total involuting mammary gland (RNA) but was 10-fold (protein) overexpressed in the alveolar cell lineage and not overexpressed in the ductal cell lineage. In other cases it is likely that a 2-fold increase could be biologically meaningful *in vivo*. For example, we detected a 2.0-fold increase in the M6P/IGF2R, an imprinted gene in rodents (52), suggesting that a 2-fold difference in its expression has been evolutionarly selected and conserved.

Both the induced YWK-II expression and repressed neuroligin 1 expression could play a role in tumor regression through a differentiation process. YWK-II, a transmembrane protein, is expressed in the mammary gland (data not shown) and has been shown to be a marker for differentiation of spermatogonia (53). It modulates cell-cell adhesion, as in sperm-egg adhesion during fertilization (54). Also, the polypeptide sequences of the YWK-II transmembrane and cytoplasmic domains are 70.6% homologous to the same domains of the human A4 amyloid protein found in brain plaques of Alzheimer disease patients (39). Differential gene expression of the A4 amyloid gene is associated with retinoic acid-induced morphologic differentiation of neurite processes in two model systems; the A4 amyloid mRNA is induced 34-fold in retinoid-treated P19

embryonal carcinoma cells (55) and 10-fold in retinoid-treated SH-SY5Y neuroblastoma cells (56). Neuroligin 1 is a neuronal cell surface protein found enriched in synaptic plasma membranes and binds to brain specific β-neurexins as a ligand. Expression of nueroligin 1 was tested in various tissues, but was restricted to brain tissue (45). Therefore, neuroligin 1 expression in mammary carcinomas may reflect deregulated gene expression. Interestingly as carcinomas regressed, neuroligin 1 expression was repressed or turned off, which is consistent with regulated gene expression in most normal tissue.

The SD screen was applied to monoterpene-treated mammary carcinomas resected at mid-regression. Therefore, the identified MIG/MRG cDNAs reflect differential gene expression patterns consistent with apoptosis and differentiation of actively regressing carcinomas. In order to better understand the process by which monoterpenes first initiate tumor regression, we are currently identifying early MIG/MRG cDNAs using SD on mammary carcinomas treated with monoterpenes for 24 hours.

In summary, the observed alterations in gene expression help to better define the process associated with monoterpene-mediated tumor regression. Although the data presented correlate monoterpene-treatment, induction of TGFβ signaling components, and tumor regression, the data do not show that TGFβ signalling is a causal event in monoterpene-mediated tumor regression. It is, however, consistent with our working hypothesis that monoterpenes promote the upregulation of the M6P/IGF2R, thereby causing increased levels of activated TGFβ1 available for ligand binding to the upregulated TGFβIIR and initiating mitoinhibitory and apoptotic signalling. We are currently investigating this hypothesis by evaluating whether the M6P/IGF2R upregulation is the central causal event that triggers tumor regression.

REFERENCES

1. Crowell, P. L., and Gould, M. N. (1994) *Crit Rev Oncog* **5**(1), 1-22
2. Gould, M. N. (1995) *J Cell Biochem Suppl* **22**, 139-44
3. Crowell, P. L., Kennan, W. S., Haag, J. D., Ahmad, S., Vedejs, E., and Gould, M. N. (1992) *Carcinogenesis* **13**(7), 1261-4
4. Elegbede, J. A., Elson, C. E., Qureshi, A., Tanner, M. A., and Gould, M. N. (1984) *Carcinogenesis* **5**(5), 661-4
5. Elson, C. E., Maltzman, T. H., Boston, J. L., Tanner, M. A., and Gould, M. N. (1988) *Carcinogenesis* **9**(2), 331-2
6. Haag, J. D., Lindstrom, M. J., and Gould, M. N. (1992) *Cancer Res* **52**(14), 4021-6
7. Haag, J. D., and Gould, M. N. (1994) *Cancer Chemother Pharmacol* **34**(6), 477-83
8. Maltzman, T. H., Hurt, L. M., Elson, C. E., Tanner, M. A., and Gould, M. N. (1989) *Carcinogenesis* **10**(4), 781-3
9. Gould, M. N., Moore, C. J., Zhang, R., Wang, B., Kennan, W. S., and Haag, J. D. (1994) *Cancer Res* **54**(13), 3540-3
10. Russin, W. A., Hoesly, J. D., Elson, C. E., Tanner, M. A., and Gould, M. N. (1989) *Carcinogenesis* **10**(11), 2161-4
11. McNamee, D. (1993) *Lancet* **342**, 801
12. Shi, W., and Gould, M. N. (1995) *Cancer Lett* **95**(1-2), 1-6
13. Crowell, P. L., Chang, R. R., Ren, Z. B., Elson, C. E., and Gould, M. N. (1991) *J Biol Chem* **266**(26), 17679-85
14. Crowell, P. L., Ren, Z., Lin, S., Vedejs, E., and Gould, M. N. (1994) *Biochem Pharmacol* **47**(8), 1405-15
15. Gelb, M. H., Tamanoi, F., Yokoyama, K., Ghomashchi, F., Esson, K., and Gould, M. N. (1995) *Cancer Lett* **91**(2), 169-75
16. Ren, Z., and Gould, M. N. (1994) *Cancer Lett* **76**(2-3), 185-90
17. Kato, K., Cox, A. D., Hisaka, M. M., Graham, S. M., Buss, J. E., and Der, C. J. (1992) *Proc Natl Acad Sci USA* **89**, 6403
18. Dennis, P. A., and Rifkin, D. B. (1991) *Proc Natl Acad Sci USA* **88**(2), 580-4
19. Jirtle, R. L., Haag, J. D., Ariazi, E. A., and Gould, M. N. (1993) *Cancer Res* **53**(17), 3849-52
20. Wang, Z., and Brown, D. D. (1991) *Proc Natl Acad Sci USA* **88**(24), 11505-9
21. Liang, P., and Pardee, A. B. (1992) *Science* **257**(5072), 967-71
22. Mou, L., Miller, H., Li, J., Wang, E., and Chalifour, L. (1994) *Biochemical & Biophysical Research Communications* **199**(2), 564-9
23. Hadman, M., Adam, B. L., Wright, G. L., Jr., and Bos, T. J. (1995) *Analytical Biochemistry* **226**(2), 383-6
24. Callard, D., Lescure, B., and Mazzolini, L. (1994) *Biotechniques* **16**(6), 1096-7, 1100-3

25. Liang, P., Averboukh, L., and Pardee, A. B. (1993) *Nucleic Acids Res* **21**(14), 3269-75
26. Liang, P., Bauer, D., Averboukh, L., Warthoe, P., Rohrwild, M., Muller, H., Strauss, M., and Pardee, A. B. (1995) *Methods Enzymol* **254,** 304-21
27. Liang, P., and Pardee, A. B. (1995) *Curr Opin Immunol* **7**(2), 274-80
28. Zhao, S., Ooi, S. L., and Pardee, A. B. (1995) *Biotechniques* **18**(5), 842-6, 848, 850
29. Bertioli, D. J., Schlichter, U. H., Adams, M. J., Burrows, P. R., Steinbiss, H. H., and Antoniw, J. F. (1995) *Nucleic Acids Research* **23**(21), 4520-3
30. Ariazi, E. A., and Gould, M. N. (1996) *BioTechniques* **20,** 446-51
31. Sanguinetti, C. J., Dias Neto, E., and Simpson, A. J. (1994) *Biotechniques* **17**(5), 914-21
32. Altschul, S. F., Gish, W., Miller, W., Myers, E. W., and Lipman, D. J. (1990) *Journal of Molecular Biology* **215**(3), 403-10
33. Araki, N., Robinson, F. D., and Nishimoto, S. K. (1993) *Journal of Bone & Mineral Research* **8**(3), 313-22
34. Debuire, B., Sol, O., Lemoine, A., and May, E. (1995) *Clinical Chemistry* **41**(6 Pt 1), 819-25
35. Gebhardt, A., Peters, A., Gerding, D., and Niendorf, A. (1994) *Journal of Lipid Research* **35**(6), 976-81
36. Kawaguchi, H., Yavari, R., Stover, M. L., Rowe, D. W., Raisz, L. G., and Pilbeam, C. C. (1994) *Endocrine Research* **20**(3), 219-33
37. Mularoni, A., Beck, L., Sadir, R., Adessi, G. L., and Nicollier, M. (1995) *Biochemical & Biophysical Research Communications* **217**(3), 1105-11
38. Zhao, J., Araki, N., and Nishimoto, S. K. (1995) *Gene* **155**(2), 159-65
39. Yan, Y. C., Bai, Y., Wang, L. F., Miao, S. Y., and Koide, S. S. (1990) *Proc Natl Acad Sci USA* **87**(7), 2405-8
40. McKanna, J. A. (1995) *Anatomical Record* **242**(1), 1-10
41. Wrana, J. L., Attisano, L., Carcamo, J., Zentella, A., Doody, J., Laiho, M., Wang, X. F., and Massague, J. (1992) *Cell* **71**(6), 1003-14
42. Wrana, J. L., Attisano, L., Wieser, R., Ventura, F., and Massague, J. (1994) *Nature* **370**(6488), 341-7
43. Carcamo, J., Zentella, A., and Massague, J. (1995) *Mol Cell Biol* **15**(3), 1573-81
44. Chen, R. H., Moses, H. L., Maruoka, E. M., Derynck, R., and Kawabata, M. (1995) *J Biol Chem* **270**(20), 12235-41
45. Ichtchenko, K., Hata, Y., Nguyen, T., Ullrich, B., Missler, M., Moomaw, C., and Sudhof, T. C. (1995) *Cell* **81**(3), 435-43
46. Kovacina, K. S., Steele-Perkins, G., Purchio, A. F., Lioubin, M., Miyazono, K., Heldin, C. H., and Roth, R. A. (1989) *Biochemical & Biophysical Research Communications* **160**(1), 393-403
47. Kornfeld, S. (1992) *Annual Review of Biochemistry* **61,** 307-30

48. De Souza, A. T., Hankins, G. R., Washington, M. K., Fine, R. L., Orton, T. C., and Jirtle, R. L. (1995) *Oncogene* **10**(9), 1725-9
49. De Souza, A. T., Hankins, G. R., Washington, M. K., Orton, T. C., and Jirtle, R. L. (1995) *Nat Genet* **11**(4), 447-9
50. Sue, S. R., Chari, R. S., Kong, F. M., Mills, J. J., Fine, R. L., Jirtle, R. L., and Meyers, W. C. (1995) *Ann Surg* **222**(2), 171-8
51. Filmus, J., and Kerbel, R. S. (1993) *Curr Opin Oncol* **5**(1), 123-9
52. Barlow, D. P., Stöger, R., Hermann, B. G., Saito, K., and Schweifer, N. (1991) *Nature* **349**, 84-7
53. Yan, Y. C., Miao, S. Y., Zong, C., Li, Y. H., Wang, L. F., and Koide, S. S. (1992) *Archives of Andrology* **28**(1), 1-6
54. Vanage, G., Lu, Y. A., Tam, J. P., and Koide, S. S. (1992) *Biochemical & Biophysical Research Communications* **183**(2), 538-43
55. Fukuchi, K., Deeb, S. S., Kamino, K., Ogburn, C. E., Snow, A. D., Sekiguchi, R. T., Wight, T. N., Piussan, H., and Martin, G. M. (1992) *Journal of Neurochemistry* **58**(5), 1863-73
56. Konig, G., Masters, C. L., and Beyreuther, K. (1990) *FEBS Letters* **269**(2), 305-10

FOOTNOTES

[1] The abbreviations used are: DMBA, 7,12-dimethylbenz[*a*]anthracene; NMU, *N*-methyl-*N*-nitrosourea; CoQ, ubiquinone; TGFβ1, transforming growth factor β1; M6P/IGF2R, mannose 6-phospate/insulin-like growth factor II receptor; IGF2, insulin-like growth factor II; PCR, polymerase chain reaction; SD, subtractive display; MIG, monoterpene-induced gene; MRG, monoterpene-repressed gene; RT-PCR, reverse transcriptase-PCR; LC1, lipocortin 1; TGFβIIR, transforming growth factor β type II receptor; COXII, cytochrome c oxidase subunit II; YWK-II, sperm membrane protein YWK-II; Y89, 5' end similar to YWK-II; RPA, RNase Protection Assay.

[2] Bailey, H. and Gould, M. N., personal communication.

TABLE I

Competitive RT-PCR primers and product sizes

Primer sequences for competitive RT-PCR and respective product sizes are shown. In order to achieve sufficient agarose gel resolution of all 4 PCR products for each competitive RT-PCR experiment, G3PDH MIMIC 1 was used in the LC1 competitive RT-PCR reactions while G3PDH MIMIC 2 was used in the TGFβIIR and neuroligin 1 competitive RT-PCR reactions. MIMIC sequences reflect only the 3' end of the composite primer used in the 1° PCR reactions during MIMIC construction to amplify from the heterologous DNA, and the 5' end of the composite primers are given by each respective target gene primer sequence.

Target DNA	Primers (5'-3')	Product Size (bp)
LC1	5' CCCTACCCTTCCTTCAATC 3' TGGCTTCATACAGTTTCTCAG	745
LC1 MIMIC	5' TGTTATACAGGGAGATGAAA 3' TTGAGTCCATGGGGAGCTTT	414
TGFβIIR	5' GCCAACAACATCAACCACAAT 3' GGGGCTCATAATCTTTCACTTCTC	724
TGFβIIR MIMIC	5' CGCAAGTGAAATCTCCTCCG 3' TTTCATCTCCCTGTATAACA	245
neuroligin 1	5' GAATAACGAGGGAGGGGGAGGTGGAT 3' CCGCTGGAGAAAGATGGAATGGTGGTA	526
neuroligin 1 MIMIC	5' CGCAAGTGAAATCTCCTCCG 3' CAATCAGCTCACGAAACTTG	193
G3PDH	5' TGAAGGTCGGTGTCAACGGATTTGGC 3' CATGTAGGCCATGAGGTCCACCAC	983
G3PDH MIMIC 1	5' CGCAAGTGAAATCTCCTCCG 3' TTGAGTCCATGGGGAGCTTT	604
G3PDH MIMIC 2	5' CGCAAGTGAAATCTCCTCCG 3' TCTGTCAATGCAGTTTGTAG	450

TABLE II

Isolated MIG/MRG clones

Identified Monoterpene-Induced Genes (MIG)

Clone	Gene Identity
MIG-3 / MIG-9 / MIG-21 MIG-23 / MIG-24 / MIG-27	cytochrome c oxidase subunit II (COX II)
MIG-12	lipocortin 1 (LC1)
MIG-19	calmodulin (RCM3)
MIG-30 / MIG-32 / MIG-34 MIG-35/ MIG-53 / MIG-54 / MIG-55	sperm membrane protein (YWK-II)
MIG-33	transforming growth factor-β type II receptor (TGFβIIR)
MIG-38	calcium transporting ATPase (SERCA I)
MIG-42	mannose 6-phosphate/ insulin-like growth factor II receptor (M6P/IGF2R)
MIG-51	fast myosin alkali light chains MLC1-f and MLC3-f
MIG-59 / MIG-60	cDNA clone Y89 5' end similar to YWK-II

33 MIG clones are unidentified

Identified Monoterpene-Repressed Genes (MRG)

Clone	Gene Identity
MRG-31	neuroligin 1

57 MRG clones are unidentified

TABLE III

Confirmed MIG/MRG differential expression

The differential expression of selected MIG/MRG known cDNAs was confirmed by the indicated method. RPA indicates an RNA Protection Assay was used to quantitate expression. Neuroligin 1 was repressed in 1/5 or not detected (ND) in 4/5 monoterpene-treated regressing carcinomas. P values were calculated by Student's *t* test.

Gene	Fold Induction/Repression	Quantitation Method
M6P/IGF2R	2.0-Fold Induced ($P \leq 0.002$)	RPA (Data from 19)
YWK-II	2.9-Fold Induced ($P \leq 0.00006$)	Northern blot
LC1	2.9-Fold Induced ($P \leq 0.00003$)	Competitive RT-PCR
TGFβIIR	3.1-Fold Induced ($P \leq 0.0002$)	Competitive RT-PCR
neuroligin 1	8.8-Fold Repressed (1/5); ND (4/5)	Competitive RT-PCR

FIG. 1. **Flowchart of the Subtractive Display Methodology.** cDNA libraries are generated from matched tissues and designated +cDNA (monoterpene-treated) and -cDNA (control, non-treated). cDNA (solid box) is fragmented with restriction endonucleases and ligated to symmetrical linkers (hatched boxes) for PCR amplification. +cDNA and -cDNA are subjected to multiple rounds of subtractive hybridization and PCR amplification to enrich for both induced and repressed genes. Subtracted libraries are reconfigured by subcloning into a trimming vector and subjected to 3 cycles of precise, unidirectional trimming which serves to randomize DNA sequence (stipled box) and provide a different linker on one end of the cDNA fragments (cross-hatched box) or asymmetric linkers. Subtracted, reconfigured cDNA libraries are PCR-display using 16 sets of primers including 1 fixed primer and 1 of 16 subpopulation primers. The subpopulation primer overlaps the cDNA insert by 2-bases (designated by NN), which selects for amplification of a subset of cDNAs.

FIG. 2. **PCR Product Display During the Subtractive Hybridization Process.** A subpopulation of the cDNA libraries was selectively amplified using a primer of sequence 5'-CTTGCTTGAATTCGGACTA(A/T)(G/C)-3', which anneals at both ends of the cDNA fragments and overlaps two bases of the cDNA insert. Lanes alternate monoterpene-treated regressing (+) and control non-regressing (-) carcinoma derived cDNA. Beginning on the left, lanes labelled + and - are cDNAs before subtraction, and the numbered lanes toward the right are cDNAs after each consecutive round of subtraction. The arrow indicates the band identified as the YWK-II gene. PCR products were labelled with [α-^{35}S] dATP and resolved on a 5% polyacrylamide sequencing gel and visualized on X-ray film.

FIG. 3. **Schematic of a cDNA Fragment and Primers Used in Subtractive Display.** The schematic represents a cDNA fragment processed through 6 rounds of subtractive hybridization and 3 cycles of trimming ($\pm$6Δ3 cDNA). The unique linker sequences at each end of the cDNA fragment are boxed; the bold sequence in the right linker is an *Eco*RI recognition site. The shaded region of the cDNA insert represents 2 randomized base pairs, after trimming, which overlap the 2 bases (NN) at the 3' end of the subpopulation primer.

FIG. 4 **Optimization of Subtractive Display.** cDNA libraries processed through 6 rounds of subtraction and 3 cycles of trimming (6Δ3 subtracted cDNA) were PCR-amplified in the presence of [α-^{35}S] dATP using the fixed primer along with the AC, AG, or GA (sequence specifies the 2 bases at the 3' end) subpopulation primers, as indicated. Lanes alternate monoterpene-treated regressing (+) and control non-regressing (-) carcinoma derived cDNA. Annealing of primers was carried out at 63° C, 61° C, 59° C, and 57° C using dNTP concentrations

of either 10 μM or 20 μM, as indicated. Labelled PCR products were resolved on a 5 % polyacrylamide sequencing gel and visualized on a PhosphorImager.

FIG. 5 **Subtractive Display Using All 16 Subpopulation Primer Sets.** cDNA libraries processed through 6 rounds of subtraction and 3 cycles of trimming (6Δ3 subtracted cDNA) were PCR-amplified in the presence of [α-^{35}S] dATP using the fixed primer along with each of the 16 subpopulation primers; the subpopulation primer used, specified by the 2-base sequence at the 3' end of the primer, is indicated above each lane. Lanes alternate monoterpene-treated regressing (+) and control non-regressing (-) carcinoma derived cDNA. Annealing of primers was carried out at 59° C using 20 μM dNTP. The arrow indicates one of the bands that identified the YWK-II gene. Labelled PCR products were resolved on a 5 % polyacrylamide sequencing gel and visualized on a PhosphorImager.

FIG. 6 **LC1 (MIG-12) RNA Expression Using Competitive RT-PCR.** *A*, The differential expression of LC1 between a panel of control non-regressing (lanes labelled CON1-CON5) and 10% limonene-treated regressing (lanes labelled LIM1-LIM5) carcinomas was demonstrated by competitive RT-PCR. PCR products corresponding to G3PDH, LC1, G3PDH MIMIC, and LC1 MIMIC and their respective sizes (in bp) are indicated. PCR primers were 5'-labelled with fluorescein; products were resolved on a 2% agarose gel and visualized on a FluorImager. *B*, LC1 was induced 2.9-fold in 10% limonene-treated regressing carcinomas compared to control non-regressing carcinomas. The LC1 expression was quantified from the gel in panel A. by first normalizing the LC1 and G3PDH bands to their respective MIMICs and second by normalizing LC1 to G3PDH.

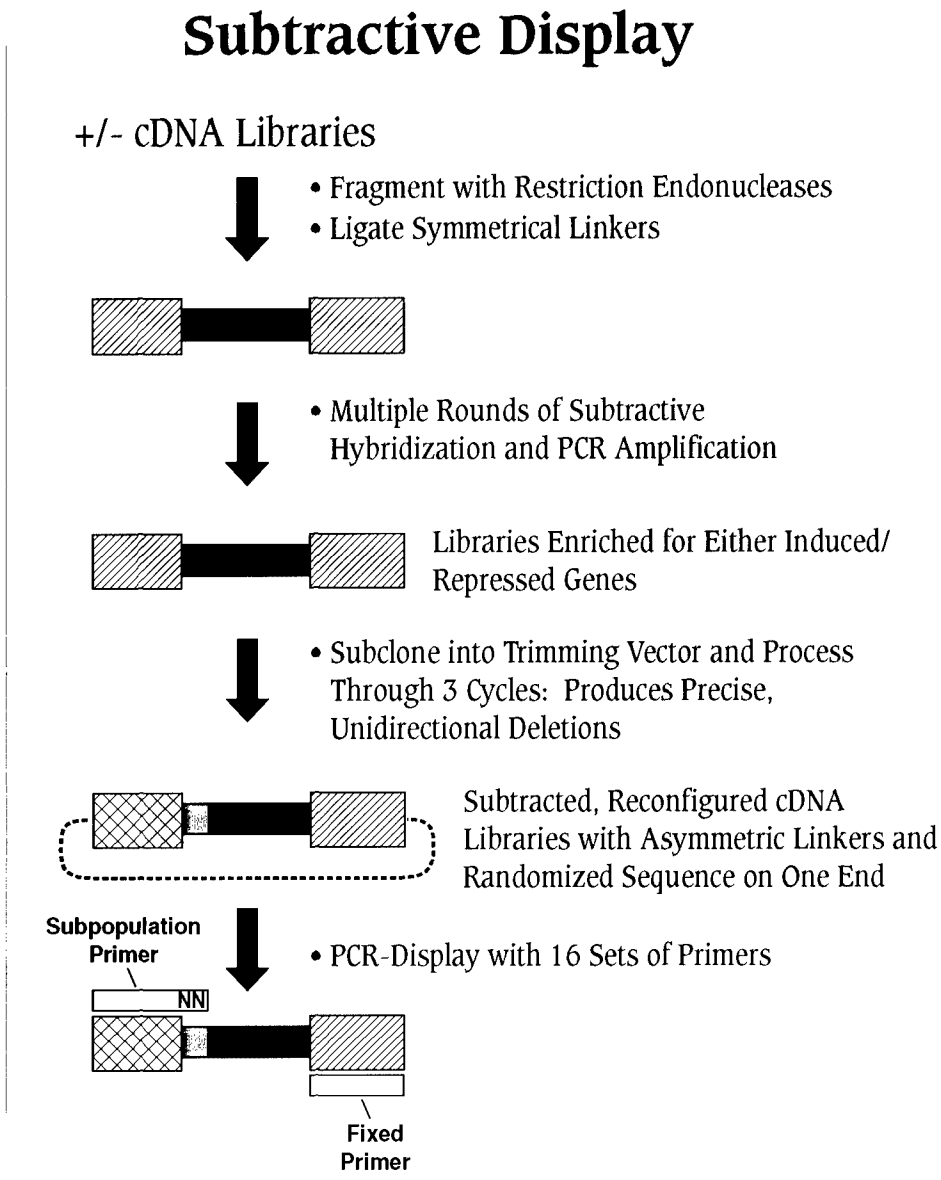
Subtractive Display
+/- cDNA Libraries
• Fragment with Restriction Endonucleases
• Ligate Symmetrical Linkers
• Multiple Rounds of Subtractive Hybridization and PCR Amplification
Libraries Enriched for Either Induced/ Repressed Genes
• Subclone into Trimming Vector and Process Through 3 Cycles: Produces Precise, Unidirectional Deletions
Subtracted, Reconfigured cDNA Libraries with Asymmetric Linkers and Randomized Sequence on One End
Subpopulation Primer
NN
• PCR-Display with 16 Sets of Primers
Fixed Primer

FIG. 1

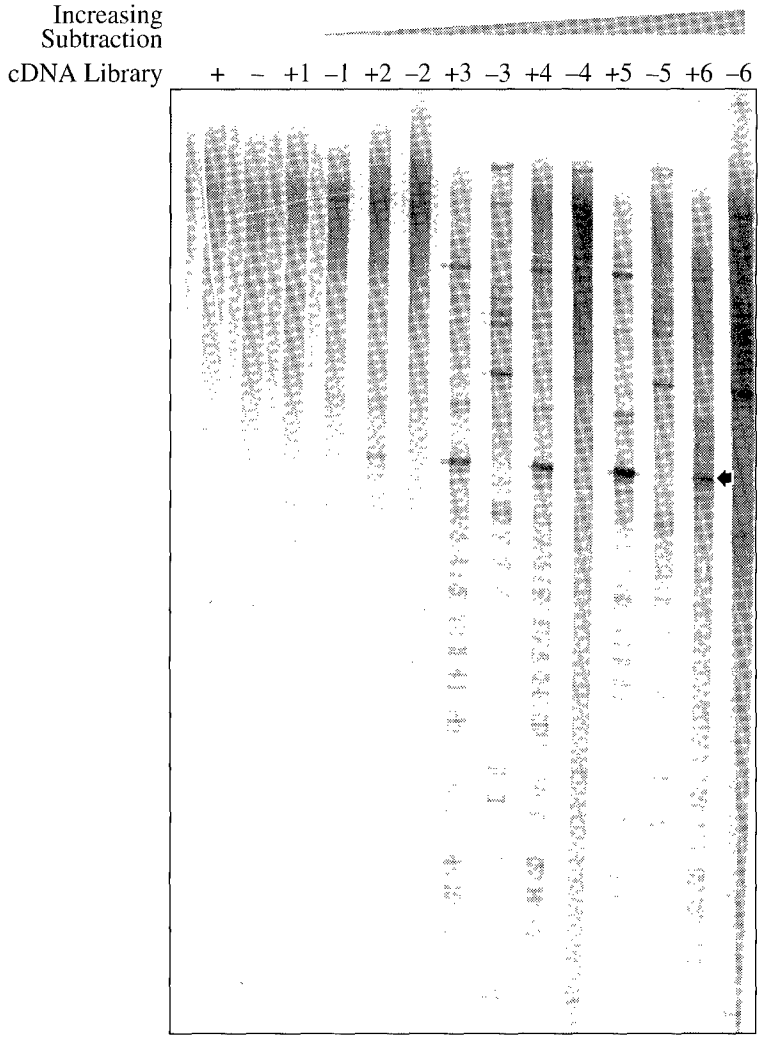

FIG. 2

Subtracted, Reconfigured cDNA Library + Subpopulation PCR Primer Set

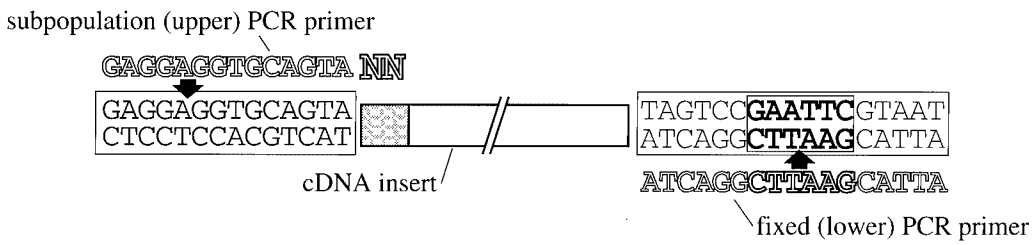

FIG. 3

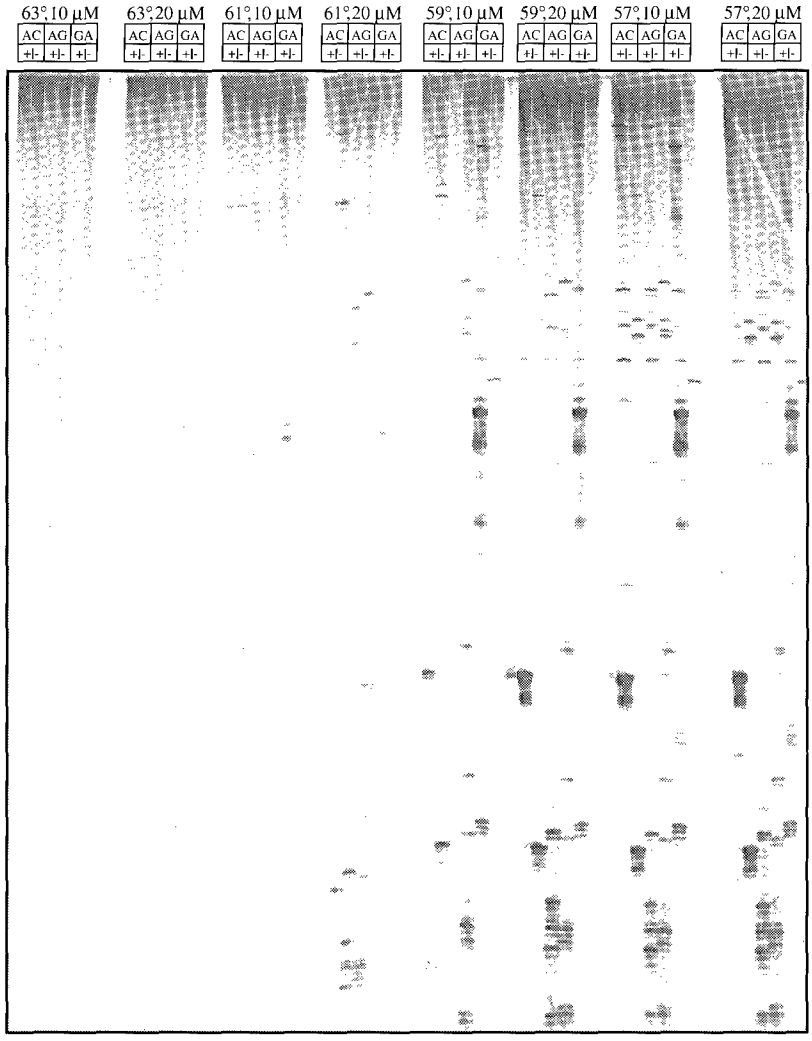
63°,10 µM
63°,20 µM
61°,10 µM
61°,20 µM
59°,10 µM
59°,20 µM
57°,10 µM
57°,20 µM
AC AG GA
+/- +/- +/-

FIG. 4

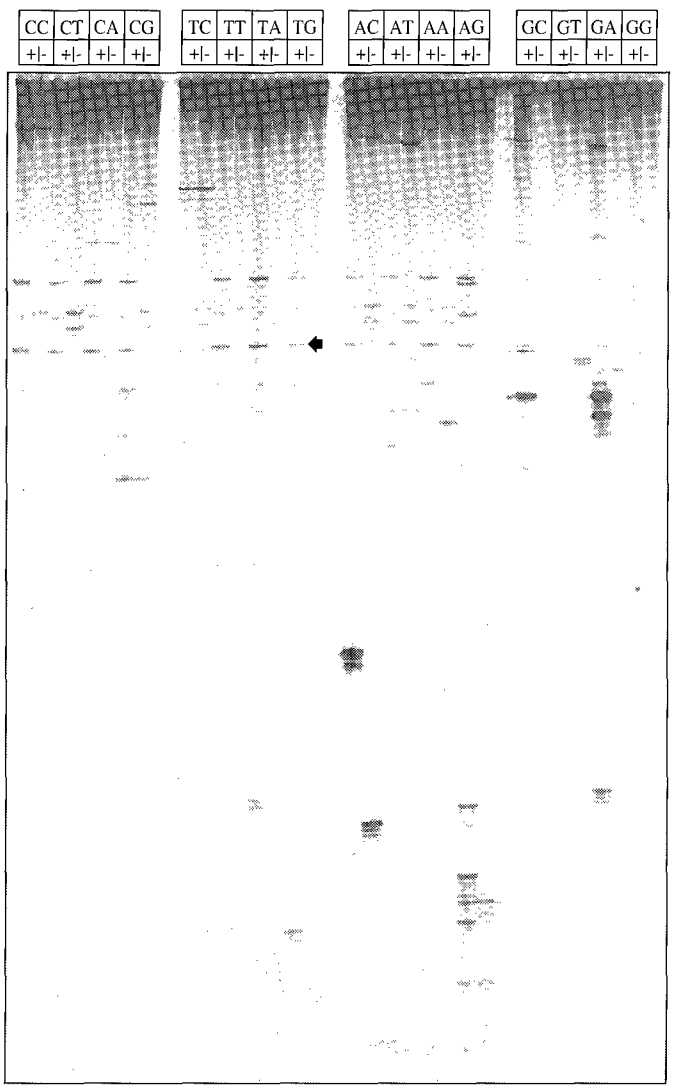

FIG. 5

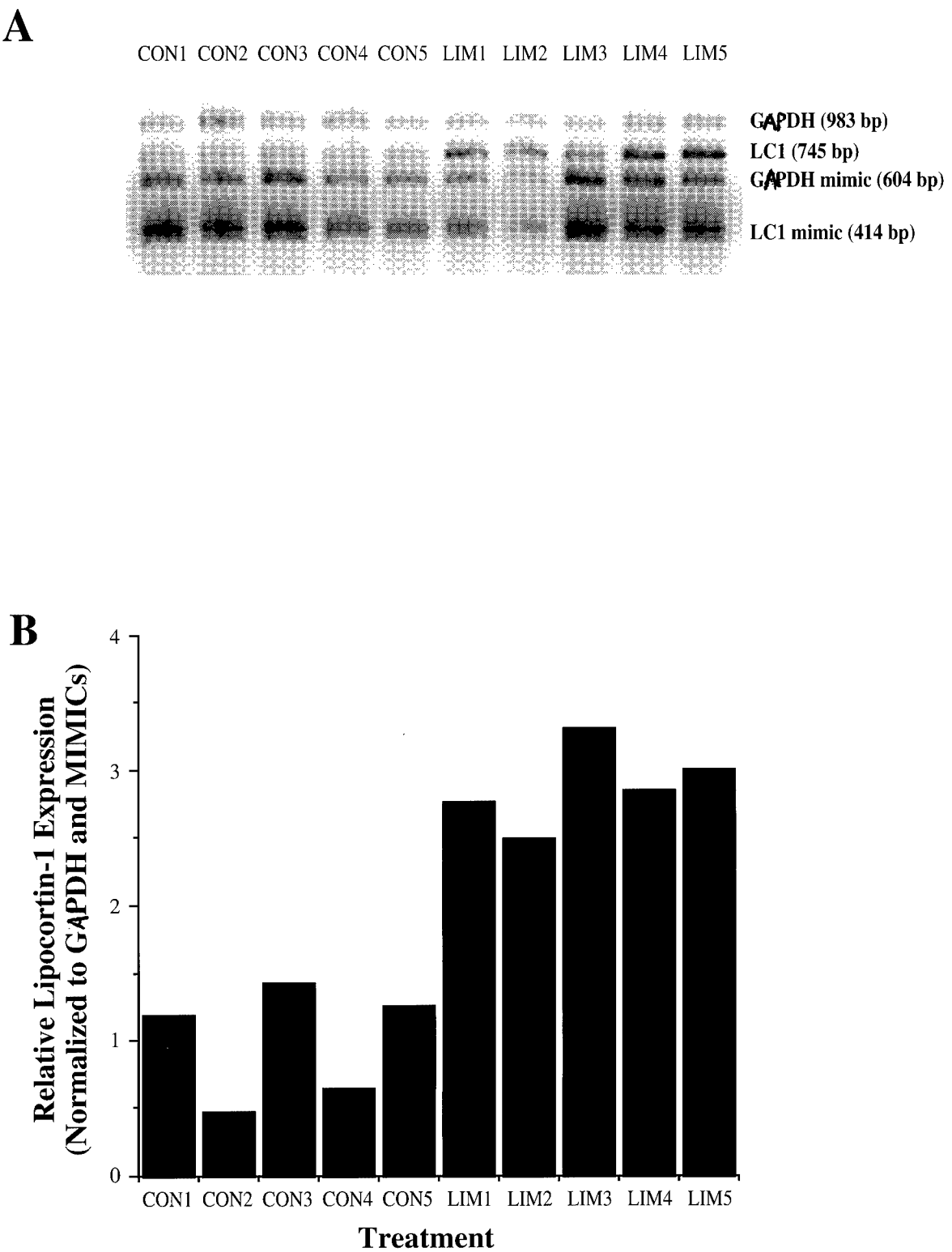
A
CON1 CON2 CON3 CON4 CON5 LIM1 LIM2 LIM3 LIM4 LIM5
GAPDH (983 bp)
LC1 (745 bp)
GAPDH mimic (604 bp)
LC1 mimic (414 bp)
B
Relative Lipocortin-1 Expression
(Normalized to GAPDH and MIMICs)
0
1
2
3
4
CON1 CON2 CON3 CON4 CON5 LIM1 LIM2 LIM3 LIM4 LIM5
Treatment

FIG 6

Appendix: Supplement to DAMD17-94-J-4041

Title: Histopathologic Alterations, Cytostasis and Apoptosis in Monoterpene-Treated, Regressing Rat Mammary Carcinomas

ABSTRACT

We investigated cellular alterations involved with monoterpene-treated mammary carcinoma regression. In the regressing tumors, the dense anaplastic epithelial compartment was deleted and replaced by stroma. The remaining carcinoma cells aggregated to form lumen-like structures. There was no significant infiltration of monocytes/macrophages, mast cells or lymphocytes, nor was inflammation observed. Cellular proliferation of monoterpene-treated, regressing carcinomas were significantly inhibited as determined by *in vivo* BrdU labelling. Ultrastructural criteria and *in situ* terminal deoxynucleotidyl transferase-mediated dUTP nick end-labeling showed apoptosis was significantly induced in the monoterpene-treated regressing carcinomas. Actin microfilaments accumulated as aggregates during monoterpene-induced regression of carcinomas. However, actin did not aggregate in the subset of monoterpene-treated, non-regressing carcinomas, but actin aggregates accumulated during mammary gland involution. Thus, formation of actin aggregates was associated with apopotosis and not monoterpene-treatment.

Chemotherapeutic agents can be grouped into two broad classes. One class of chemotherapeutic agents typically interfere with the ability of cells to replicate DNA by acting as antimetabolites, topoisomerase inhibitors, and alkylating agents. A second class of chemotherapeutic agents interfere with cell division such as the plant alkaloids. Although the chemotherapeutics are targeted for neoplastic tissue, they often exhibit a low thereapuetic ratio due to normal tissue toxicity, thus limiting dosage. The naturally occurring monoterpenes limonene (LIM) and perillyl alchohol (POH) have been shown to be effective chemopreventive and chemotherapeutic agents in rodent organ-specific tumor models (reviewed in (1,2). Our laboratory has extensively characterized the anti-cancer activities of monoterpenes in the chemical carcinogen dimethylbenz-[*a*]-anthracene (DMBA)- and *N*-methyl-*N*-nitrosourea (NMU)-induced rat mammary carcinoma models (3-8). Dietary administration of 10% LIM or 2% POH caused the complete regression of ~66% advanced DMBA - or NMU - induced carcinomas (6,7). Furthermore, the only toxicity observed during treatment was initial weight loss due to food aversion (6,7). Because of the high efficacy and low toxicity of monoterpenes for chemoprevention and chemotherapy, phase I clinical trials are being conducted using LIM in England (9) and POH in the United States (personal communication, Bailey, H. and Gould, M. N.).

Morphology of monoterpene-treated regressing mammary carcinomas indicates regression is a dramatic differentiation/remodeling process. Regressing carcinomas exhibit dense cords of anaplastic epithelium charasteristic of rat mammary carcinomas and regions of shrinking anaplastic epithelium. Regressing carcinomas do not show inflammation, necrosis or lymphocyte involvement (6).

Several biochemical and cellular activities are associated with monoterpene-mediated carcinoma regression including selective inhibition of 21-26 kD small G proteins (10-12) and inhibition of ubiquinone synthesis (13). Investigations into gene expression demonstrated that the mannose 6-phosphate/insulin-like growth factor type II receptor (M6P/IGF2R), which both facillitates latent-TGFβ1 activation and degrades the mammary mitogen insulin-like growth factor II (IGF2) (14), and the mitoinhibitory transforming growth factor β1 (TGFβ1) were significantly induced in actively regressing carcinomas as shown by immunohistochemistry (15). Investigations into gene expression were further explored by screening 10% LIM-treated, actively regressing advanced rat mammary carcinomas using subtractive display (SD) (Ariazi and Gould, manuscript in press). Identified cDNAs, termed monoterpene-induced genes (MIG) and monoterpene-repressed genes (MRG), were consistent with a differentiation/remodeling process of tumor regression. The SD screen again identified the M6P/IGF2R, induced 2.0-fold, as well as the transforming growth factor β type II receptor (TGFβIIR), induced 3.1-fold. Induction of the M6P/IGF2R and TGFβIIR suggested these signalling pathways promote inhibition of cellular proliferation and/or apoptosis in order to effect tumor regression. Suggestive of an apoptotic

, process, the SD screen identified a marker of apoptosis for the involuting mammary gland, lipocortin 1 (LC1) (16) which was induced 2.9-fold. (Ariazi and Gould, manuscript in press).

To better characterize the cellular and morphologic alterations taking place in monoterpene-treated regressing mammary carcinomas, we analyzed the histopathology, cellular proliferation and apoptosis induuction of these regressin tumors. Initially, remodeling or morphologic differentiation was investigated. Light and electron microscopy studies of regressing mammary carcinomas showed remodeling of a shrinking epithelial compartment into lumen-like structures surrounded by a growing connective tissue compartment, similar to the architecture of a normal mammary gland. The potential cytostatic effects downstream of the M6P/IGF2R and TGFβIIR were investigated by labelling cells synthesizing DNA with bromo-deoxyuridine (BrdU). The regressing carcinomas displayed a large inhibition of cellular proliferation relative to control carcinomas. Because of the differential expression of LC1, apoptosis was directly investigated during tumor regression by morphologic analysis using electron microscopy and employing the *in situ* terminal deoxynucleotidyl transferase (TdT) - mediated dUTP nick end-labeling (TUNEL) method. Both studies showed a significantly large increase of apoptotic cells in monoterpene-treated regressing carcinomas. In addition, cells actively undergoing apoptosis presented aggregates of actin microfilaments, a potential by-product of apoptosis, which persisted after cell corpses were cleared.

Experimental Procedures

Generation of Mammary Carcinomas and Tissue Collection. Regressing (monoterpene-treated) and non-regressing (control, not-treated) carcinomas for all studies were generated by the following protocol. Virgin female Wistar-Furth rats at 50-55 days of age were administered a single dose of DMBA (50 mg/kg body weight) by gastric intubation. All rats were palpated weekly until advanced mammary carcinomas developed, defined as being $\geq$ 10 mm in diameter, at which time the rats were randomized to either a monoterpene diet or a pair-fed control diet . Monoterpenes were fed to rats at isoeffective doses of either 10% limonene (w/w) or 2% perillyl alcohol (w/w) (6,7). Carcinomas in rats on monoterpene diet that regressed to 50% of their maximum diameter were resected and defined as regressing carcinomas. Control carcinomas in the pair-fed non-treated rats were resected at the time a corresponding regressing carcinoma was resected or if the control carcinoma grew an additional 5 mm in diameter. All remaining carcinomas were collected at 15 weeks after diet randomization. All animal use was in compliance with NIH guidelines for humane care and was approved by the University of Wisconsin-Madison Medical Center Animal Use Committee.

Light and Confocal microscopy. Collected carcinomas were fixed with freshly prepared 4% paraformaldehyde in phosphate buffered saline (PBS) at pH 7.2 for 3 hrs, dehydrated in a graded series of alcohol and embedded in paraffin. All tissue sections (5 μm each) were mounted on poly-L-lysine-coated slides, deparaffinized with xylenes, rehydrated in a graded series of alcohol and stained with hematoxylin and eosin (H&E), unless otherwise stated. Histopathologic analysis of tissues involved use of an Olympus BX50 Light Microscope (Olympus, Lake Success, NY, USA) and a Bio-Rad MRC-600 Laser Scanning Confocal Microscope (Bio-Rad, Hercules, CA, USA), both of which were equipped with the relevant epifluorescence filters.

Monocyte/Macrophage and Mast Cell Staining. Monocyte/macrophages were immunohistochemically stained using an anti-ED1 antibody (Serotec, Washington, DC, USA), following manufacturer's protocol. The anti-ED1 antibody was detected using biotinylated anti-mouse IgG antibody (rat adsorbed, made in horse; Vector Laboratories, Burlingame, CA, USA), an avidin-peroxidase reaction kit (Vectastain ABC kit, Vector Laboratories), and the brown chromogen 3,3'-diaminobenzidine (DAB; Sigma, St. Louis, MO, USA). Anti-ED1 stained tissue sections were counterstained with methyl green (Sigma). Negative controls for each section were obtained by staining identical sections without the anti-ED-1 antibody. Tissue sections were stained for mast cells using acidified Toluidine blue (Sigma).

Cellular Proliferation Staining. A cell proliferation kit (Amersham Life Sciences, Arlington Heights, IL, USA) utilizing bromo-deoxyuridine (BrdU) to detect BrdU incorporated into cellular DNA was used to stain carcinoma sections from control and monoterpene treated rats. Rats were treated via an intraperitoneal injection with 1 ml of BrdU labelling reagent per kg body wt and sacrificed 2 hr after treatment or a BrdU pellet was iserted in the fat pad of the back and rats were

then sacrificed 2 days after treatment. Tissues were fixed in OmniFix II (An-Con Genetics, Melville, NY, USA) overnight and embedded in paraffin. To verify the incorporation of BrdU into cellular DNA normal mammary and intestinal tissues from each rat were also stained. Negative controls for each section were obtained by staining identical sections without the BrdU antibody. Cellular proliferation was visualized by light microscopy and quantified by counting stained nuclei in four randomly chosen fields at 200X original magnification per tissue section.

Electron Microscopy. Monoterpene-treated, regressing carcinomas and control, non-regressing carcinomas were dissected and immediately placed in 3% glutaraldehyde on dental wax. The tumors were cut into 1 mm cubes and transferred to vials with 3% glutaraldehyde in 0.1 mol/L cacodylate, pH 7.4 for 2 hr, washed 3 times with 0.1 mol/L cacodylate buffer containing 7.5% sucrose, and postfixed with 1% OsO_4 for 1.5 hr on ice. Following dehydration in a graded series of alcohol, the tissue was infiltrated with 1:1 propylene oxide:Eponate 12 (Ted Pella, Redding, CA, USA), infiltrated overnight with Eponate 12 and embedded in fresh Eponate 12. Thin sections were cut with a diamond knife on a Reichert Ultracut E ultramicrotome and stained with uranyl acetate and lead citrate. Electron micrographs were taken with an Hitachi H-7000 electron microscope operated at 75 kv.

Apoptosis Staining. An *in situ* end labeling (ISEL) or terminal deoxytransferase-mediated dUTP-end labeling (TUNEL) kit (In Situ Cell Death Detection Kit, Fluorescein, Boehringer Mannheim, Indianapolis, IN, USA) was used to visualize apoptotic nuclei (17-19). Briefly, rehydrated tissue sections were pretreated with Proteinase K, incubated with TUNEL reaction mixture [containing terminal deoxynucleotidyltransferase (TdT), dNTPs and fluorescein-conjugated dUTP) for 60 min at 37° C in a humidified chamber. Nuclei were counterstained with TO-PRO-3 (Molecular Probes, Eugene, OR, USA) for 30 min at room temperature in a humidified chamber. Tissue sections were dried at 50° C for 30 min and mounted with ProLong Antifade kit (Molecular Probes, Eugene, OR, USA).

Nuclei from TUNEL stained tissue sections were quantified on a confocal scanning microscope. Apoptosis was visualized by confocal microscopy and stained nuclei were counted in five randomly chosen fields at 600X magnification per tissue section.

Actin Cytoskeleleton Staining. Deparaffinized, rehydrated tissue sections were permeabilized with 0.1% Triton X-100 in PBS for 30 min. Actin cytoskeleton was stained with BODIPY 581/591 phallacidin (Molecular Probes) following manufacturers' protocol. Nuclei were counterstained with Hoechst 33342 (Molecular Probes) for 30 min at room temperature in a humidified chamber. Sections were dried at 50° C for 30 min and mounted with ProLong Antifade Kit (Molecular Probes).

Results

Gross Morphology and Luekocyte Status. All control, non-regressing and monoterpene-treated, regressing mammary carcinomas were stained with H&E to examine gross morphologic alterations associated with tumor regression. The control carcinomas were characterized by dense anaplastic epithelium (Fig. 1A) typical of DMBA-induced rat mammary carcinomas (20). The regressing carcinomas also displayed some regions of anaplastic epithelium but predominantly exhibited a shrinking epithelial compartment and a concomitant expanding stromal compartment (Fig. 1B). The remaining epithelial cells showed marked compaction and remodeling into lumen-like structures reminiscent of normal mammary gland (Fig. 1B). Furthermore, there was no discernible difference in gross morphology between POH- and LIM-treated regressing mammary carcinomas.

In addition to connective tissue and anaplastic epithelium, mammary tissue harbor monocytes/macrophages (21-23) and mast cells (24). Monocyte/macrophage status was determined using immunohistochemistry and the ED-1 antigen found in these cell types. Control, POH-treated, and LIM-treated tumors were stained with anti-ED-1 antibody, which was visualized using DAB, and counterstained with methyl green. Monocytes/macrophages were counted in four random 400X original magnification fields from 5 control, 5 POH-treated, and 5 LIM-treated tumors. Both control and monoterpene-treated tumors showed a large variability in quantity of monocytes/macrophages and no significant difference was found between the control and monoterpene groups. Mast cell status was determined by staining tissue sections with acidified toluidine blue. The histamine granules of mast cells preferentially stain with toluidine blue and therefore were visualized as purple, granulated cells. Mast cells were quantified using the same method as with monocytes/macrophages. There was a large variability and no significicant difference in the quantity and distribution of mast cells between the control and monoterpne-treated mammary carcinomas. Furthermore, neither inflammation nor any significant changes in lymphocyte status were observed in monoterpene-treated regressing carcinomas.

Induction of Cytostasis. Cellular proliferation was quantified in control, non-regressing and monoterpene-treated, regressing carcinomas by allowing BrdU incorportation into genomic DNA of cycling cells for either 2 hrs (data not shown) or 2 days. Tissue sections were stained for BrdU using a cell proliferation kit (Amersham). Qualitatively, the control, non-regressing carcinomas (Fig. 1A) showed a large degree of cellular proliferation as compared to an almost complete block of cellular proliferation in the monoterpene-treated, regressing carcinomas (Fig. 1B). Positive staining nuclei were counted in 4 random 200X original magnification fields. Cellular proliferation was inhibited 5.7-fold ($P<0.004$) in POH-treated and 11.0-fold ($P<0.003$) in LIM-treated regressing carcinomas as compared to control carcinomas (Fig. 2C). The difference in the degree of cytostasis between POH- and LIM-treated, regressing carcinomas was not significant. Additionally, there was no change in cellular proliferation profiles of the tumors after 2 hr as compared to 2 days of BrdU incorporation.

Ultrastructural Morphology and Induction of Apoptosis. The ultrastructural morphology of regression was investigated using electron microscopy (EM). Ultrastructural morphology suggest that the dense anaplastic epithelium of the control carcinomas was well differentiated by the presence of numerous microvilli (Fig. 3A). There was no discernable difference in ultrastructural morphology of either POH- or LIM-treated regressing carcinomas. Also, the EM confirmed the large scale remodeling of a growing stromal compartment and a shrinking epithelial compartment (Fig. 3B) whereby the epithelium morphologically differentiates into lumen-like structures (Fig. 3C).

Ultrastructural analysis revealed a mode of cell loss during tumor regression occurs via an apoptotic process. Apoptotic cells were detected using morphologic criteria of chromatin margination, cytoplasmic condensation, lucent vacuoles, loss of microvilli, nuclear compaction and fragmentation, and apoptotic bodies (reviewed in (25)). A significant increase in apoptotic cells were detected in monoterpene-treated regressing carcinomas as compared to the control carcinomas. Apoptotic cells generally resided at the periphery of epithelial cords (Fig 3B) and newly formed lumen-like structures, and were sloughed off into the lumen-like structures (Fig. 3C).

Induction of apoptosis during tumor regression was further studied by staining control and monoterpene-treated, regressing carcinomas using the TUNEL assay and was visualized by confocal microscopy (Fig 3D and 3E). The TUNEL assay preferentially stains apoptotic nuclei by tailing fluoroscein-conjugated dUTP onto the 3'-OH ends of fragmented DNA, allowing the apoptotic nuclei to appear green. Tissue sections were counterstained with the DNA intercalator TO-PRO-3 (Molecular Probes), allowing non-apoptotic nuclei to appear blue. Control carcinomas showed a low, basal level of apoptosis (Fig. 3D), as has been previously reported (26) , while the monoterpene-treated carcinomas showed a significant increase in apoptosis (Fig. 3E). Apoptosis was quantified by counting apoptotic nuclei in 5 randomly chosen fields at 600X original magnification in each treatment group. The number of apoptotic nuclei increased 12.1-fold in POH-treated regressing tumors ($P < 3 \times 10^{-9}$) and 10.4-fold in LIM-treated regressing tumors ($P < 6 \times 10^{-8}$) relative to control tumors (Fig. 3F). There was no significant difference in number of apoptotic nuclei between POH- and LIM-treated regressing carcinomas.

Accumulation of Actin Aggregates. The status of the actin cytoskeleton during regression was examined by staining tissue samples for actin microfilaments with the phallotoxin, BODIPY-581/591 phallacidin (Molecular Probes), which appears red by epifluorescence light microscopy. Nuclei were counterstained with Hoechst 33342 and appear blue. Control carcinomas display smooth, well organized actin microfilaments (Fig. 4A). However, in monoterpene-treated regressing carcinomas, actin microfilaments were accumulated into aggregates (Fig. 4B). The actin aggregates were not detected in monoterpene-treated carcinomas that failed to regress (Fig. 4C). Also, necrotic tissue in control carcinomas, as judged by swelling and subsequent degenerative autolysis, did not show accumulation of actin aggregates (Fig. 4D). Ultrastructural morphology of actin aggregates during regression was further studied by EM. A minor fraction of

actin aggregates accumulated intracellularly in apoptotic cells (Fig. 4E and 4F); however, the majority of actin aggregates accumulated extracellularly (Fig. 4G) and formed pronounced actin aggregates which persisted in newly formed lumen-like structures (Fig. 4H).

In order to assess whether monoterpene-treatment was associated with the formation of actin aggregates, normal age matched rats, not given DMBA, were treated with dietary 2% POH. Normal mammary gland from these monoterpene-treated rats was stained for actin microfilaments. The actin morphology was indistinguishable from control rats (data not shown). Next, in order to assess whether apoptosis in the mammary gland was associated with the formation of actin aggregates, actin microfilament morphology was characterized during various stages of mammary gland differentiation in normal age-matched rats not given DMBA and not treated with monoterpenes. Actin microfilaments were well organized and actin aggregates were not observed in the virgin (Fig. 5A), lactating (Fig. 5B), and pregnant (Fig. 5C) mammary glands. However, actin aggregates were observed in the involuting mammary gland (Fig. 5D). Because mammary gland involution occurs via an apoptotic process (21), actin aggregate formation was associated with apoptosis in the mammary gland.

CONCLUSIONS

Morphologic differentiation of monoterpene-treated actively regressing mammary carcinomas was investigated by light and electron microscopy studies. The large-scale remodeling process of tumor regression was characterized by reduction of the majority of epithelium, allowing the remaining epithelial cells to remodel into lumen-like structures, and a concomitant increase of stroma (Fig. 1A and 1B). The expansion of extracellular matrix may be the result of increased levels of activated TGFβ1 (27) present during monoterpene-mediated tumor regression (15). The reduction in tumor burden did not appear to be modulated by the immune system as there was no change in the status of monocytes/macrophages or mast cells during tumor regression (Fig. 1C-1F). Additionally, tumor regression does not involve inflamation nor obvious lymphocyte infiltratration.

Cytostasis was investigated by *in vivo* labelling of tumor cells synthesizing DNA with BrdU. Cellular proliferation in monoterpene-treated, regressing carcinomas was significantly inhibited 5.7-fold in 2% POH-treated and 11.0-fold in 10% LIM-treated tumors relative to control tumors (Fig. 2A-2C). Potentially, cytostasis in monoterpene-treated regressing carcinomas may be a downstream effect of the up-regulated M6P/IGF2R and TGFβIIR (Jirtle *et al*, 1993; Ariazi and Gould, manuscript in press).

A potential role for apoptosis was investigated to account for the large reduction in epithelium. Apoptosis was investigated during tumor regression by morphologic analysis using electron microscopy which showed a large increase of apoptotic cells in monoterpene-treated regressing carcinomas (Fig. 3A-3C). In addition, apoptotic nuclei were detected by employing the TUNEL method which showed apoptosis was induced 12.1-fold in 2% POH-treated and 10.4-fold in 10% LIM-treated regressing carcinomas relative to control carcinomas (Fig. 3D-3F). Consistent with reduction of tumor burden occuring via an apoptotic process, LC1, a marker of apoptosis in the involuting mammary gland (16) was up-regulated during monoterpene-mediated carcinoma regresion (Ariazi and Gould, manuscript in press). Furthermore, apoptosis is another potential effect downstream of the M6P/IGF2R and TGFβIIR signalling pathways.

Monoterpenes exhibit several biochemical effects including inhibition of isoprenylation of small G proteins. Inhibition of protein prenylation is a molecular target of several recently developed cancer therapeutics, including the peptidomimetic farnesyltransferase inhibitor L-739,749 (28). It was suggested that L-739,749 suppressed the malignant phenotype of Ras-transformed Rat1 cells by modulating Rho.(29) Rho has been shown to regulate actin stress fibers (30) and treatment of Ras-transformed Rat1 cells with L-739,749 resulted in increased actin stress fiber formation (28). Therefore, we examined the status of actin microfilaments during tumor regression. The control tumors exhibited smooth, well organized actin microfilaments (Fig. 4A) while monoterpene-treated regressing carcinomas exhibited focal areas of accumulated actin or actin aggregates (Fig. 4B). Actin aggregates were not observed in monoterpene-treated non-regressing carcinomas (Fig. 4C) nor in necrotic regions of control tumors (Fig. 4D). We

, examined the status of actin microfilaments during stages of normal mammary gland differentiation. Actin microfilament structure was well organized in the virgin, pregnant, and lactating mammary gland (Fig. 5A-5C) but formed focal actin aggregates during mammary gland involution (Fig. 5D), an apoptotic process. Noteworthy, rats that did not bear tumors but were treated with monoterpenes did not exhibit actin aggregates (data not shown). Formation of actin aggregates was therefore associated with apoptosis which occurs during mammary carcinoma regression and mammary gland involution and not with monoterpene treatment. The site of the actin aggregatation was studied by electron microscopy. The micrographs showed a minor fraction of the actin aggregates formed within apoptotic cells (Fig. 4E and 4F) but the major fraction existed extracellularly within newly formed lumen-like structures and these extracellular aggregates showed qualitatively more pronounced accumulation of actin (Fig. 4G and 4H). These data were intrepreted to mean focal actin aggregates initially form intracellularly during apoptotosis, and remain as residual bodies after the cell corpses were cleared. The actin aggregates then further accumulate within lumen-like structures as a by-product of apoptotic death. To the best of our knowledge, formation of actin aggregates during mammary carcinoma regression is a novel finding.

The differentiation/remodeling process of monoterpene-mediated carcinoma regression involves induction of M6P/IGF2R, TGFβ1 [protein only], and TGFβIIR gene expression (15); Ariazi and Gould, manuscript in press). Although we have not shown that the M6P/IGF2R and/or TGFβ signalling pathways were induced, the observed histopathology was consistent with downstream events of these pathways. The histopathology of mammary carcinoma regression indicates a large-scale deletion of the epithelium, allowing the remaining epithelial cells to remodel into lumen-like structures, and a concomitant increase of stroma. The M6P/IGF2R and/ or TGFβ signalling pathway may cause inhibition of cellular proliferation as demonstrated by BrdU staining of genomic DNA synthesis. In addition, these signalling pathway may cause an increase of apoptosis, as indicated by induced LC1 expression (Ariazi and Gould, manuscript in press) and shown by ultrasctructural morphology and TUNEL staining of genomic DNA fragmentation. Together, cytostasis and apoptosis effect carcinoma regression.

REFERENCES

1. Crowell, P. L., and Gould, M. N. (1994) *Crit Rev Oncog* **5**(1), 1-22
2. Gould, M. N. (1995) *J Cell Biochem Suppl* **22,** 139-44
3. Crowell, P. L., Kennan, W. S., Haag, J. D., Ahmad, S., Vedejs, E., and Gould, M. N. (1992) *Carcinogenesis* **13**(7), 1261-4
4. Elegbede, J. A., Elson, C. E., Qureshi, A., Tanner, M. A., and Gould, M. N. (1984) *Carcinogenesis* **5**(5), 661-4
5. Elson, C. E., Maltzman, T. H., Boston, J. L., Tanner, M. A., and Gould, M. N. (1988) *Carcinogenesis* **9**(2), 331-2
6. Haag, J. D., Lindstrom, M. J., and Gould, M. N. (1992) *Cancer Res* **52**(14), 4021-6
7. Haag, J. D., and Gould, M. N. (1994) *Cancer Chemother Pharmacol* **34**(6), 477-83
8. Maltzman, T. H., Hurt, L. M., Elson, C. E., Tanner, M. A., and Gould, M. N. (1989) *Carcinogenesis* **10**(4), 781-3
9. McNamee, D. (1993) *Lancet* **342,** 801
10. Crowell, P. L., Chang, R. R., Ren, Z. B., Elson, C. E., and Gould, M. N. (1991) *J Biol Chem* **266**(26), 17679-85
11. Crowell, P. L., Ren, Z., Lin, S., Vedejs, E., and Gould, M. N. (1994) *Biochem Pharmacol* **47**(8), 1405-15
12. Gelb, M. H., Tamanoi, F., Yokoyama, K., Ghomashchi, F., Esson, K., and Gould, M. N. (1995) *Cancer Lett* **91**(2), 169-75
13. Ren, Z., and Gould, M. N. (1994) *Cancer Lett* **76**(2-3), 185-90
14. Dennis, P. A., and Rifkin, D. B. (1991) *Proc. Natl. Acad. Sci. USA* **88**(2), 580-4
15. Jirtle, R. L., Haag, J. D., Ariazi, E. A., and Gould, M. N. (1993) *Cancer Res* **53**(17), 3849-52
16. McKanna, J. A. (1995) *Anatomical Record* **242**(1), 1-10
17. Gorczyca, W., Gong, J., and Darzynkiewicz, Z. (1993) *Cancer Res* **53**(8), 1945-51
18. Gavrieli, Y., Sherman, Y., and Ben-Sasson, S. A. (1992) *J Cell Biol* **119**(3), 493-501
19. Wijsman, J. H., Jonker, R. R., Keijzer, R., van de Velde, C. J., Cornelisse, C. J., and van Dierendonck, J. H. (1993) *J Histochem Cytochem* **41**(1), 7-12
20. Russo, J., Saby, J., Isenberg, W. M., and Russo, I. H. (1977) *J. Natl. Cancer Inst.* **59**(2), 435-445
21. Walker, N., I., Bennett, R., E., and Kerr, J. F. R. (1989) *Am. J. Anat.* **185,** 19-32
22. Lwin, K., Y., Zuccarini, O., Slaoane, J. P., and Beverly, P., C.L. (1985) *Int. J. Cancer* **36,** 433-438
23. Ferguson, D. J. P. (1985) *Virchows Arch* **407,** 369-78
24. Dabbous, M. K., Haney, L., Nicolson, G. L., Eckley, D., and Woolley, D. E. (1991) *Br. J. Cancer* **63,** 873-8
25. Kerr, J. F. R., and Searle, S. (1980) *Radiation Biology in Cancer Research* , 367-84

26. Huovinen, R., Warri, A., and Collan, Y. (1993) *Int J Cancer* **55**(4), 685-91
27. McAnulty, R. J., Chambers, R. C., and Laurent, G. J. (1995) *Biochem J* **307**(Pt 1)(Pt 1), 63-8
28. Prendergast, G. C., Davide, J. P., deSolms, S. J., Giuliani, E., Graham, S., Gibbs, J. B., Oliff, A., and Kohl, N. E. (1994) *Mol. Cell. Biol.* **14,** 4193-202
29. Lebowitz, P., F., Davide, J., P., and Prendergast, G., C. (1995) *Mol. Cell. Biol.* **15**(12), 6613-22
30. Hall, A. (1992) *Mol. Biol. Cell* **3,** 475-479

FIG. 1. **Monoterpene Effects on Gross Morphology and Immune Cell Status.** *A,* Control, non-regressing carcinoma stained with H&E showing a dense cord of anaplastic epithelium and *B,* a 2% POH-treated, regressing carcinoma stained with H&E showing a shrinking epithelial compartment remodeling into lumen-like structures and an expanding stroma. *C,* Control, non-regressing carcinoma stained by anti-ED-1 antibody immunohistochemistry showing monocytes/macrophages visualized by a brown DAB precipitate and counterstained with methyl green and *D,* a 2 % POH-treated, regressing carcinoma showing no change in monocyte/macrophage status. *E,* Control, non-regressing carcinoma stained with toluidine blue showing mast cells as metachromatic purple cells and *F,* a 2% POH-treated, regressing carcinoma showing no change in mast cell status. Tissue sections were visualized by light microscopy.

FIG. 2 **Monoterpene Inhibition of Cellular Proliferation.** *A,* Control, non-regressing carcinoma and *B,* a 2% POH-treated, regressing carcinoma showing BrdU stained nuclei (brown). Cells synthesizing DNA were labelled by BrdU incorporation over 2 days. Tissue sections visualized by light microscopy. *C,* Quantitation of BrdU stained nuclei. Cellular proliferation was inhibited 5.7-fold in 2% POH-treated ($P < 0.004$) and 11.0-fold in 10% LIM-treated ($P < 0.003$), regressing carcinomas relative to control, non-regressing carcinomas (CON n=7, 2% POH n=8, 10% LIM n=7). Nuclei were counted in four random 200X original magnification fields per tissue section. Error bars depict standard error of the mean (SEM).

FIG. 3 **Monoterpene Induction of Apoptosis.** *A,* Control, non-regressing carcinoma showing dense anaplastic epithelium. *B-C,* 2% POH-treated regressing carcinomas showing vacuolated, apoptotic cells (hollow arrows) and non-vacuolated, apoptotic cells (solid arrows), along with an expanding stroma. Apoptotic cells were frequently found on the (*B*) periphery of shrinking epithelial cords or (*C*), sloughed off into lumens. (*A-C*) Tissue sections visualized by electron microscopy. *D,* Control, non-regressing carcinoma and *E,* a 2% POH-treated, regressing carcinoma stained for apoptotic nuclei (green) and non-apoptotic nuclei (blue). Apoptotic nuclei were labelled using fluoroscein-conjugated dUTP in a TUNEL assay and non-apoptotic nuclei were counterstained with TO-PRO-3. (*D-E*) Tissue sections visualized by confocal microscopy. *F,* Quantitation of apoptosis. Apoptosis was induced 12.1-fold in 2% POH-treated ($P < 3 \times 10^{-9}$) and 10.4-fold in 10% LIM-treated ($P < 6 \times 10^{-8}$), regressing carcinomas relative to control, non-regressing carcinomas (CON n = 9, 2% POH n = 8, 10% LIM n = 8). TUNEL-stained nuclei were counted in five randomly chosen fields at 600X original magnification per tissue section. Error bars depict SEM..

FIG. 4. **Formation of Actin Aggregates During Mammary Carcinoma Regression.** *A,* Control, non-regressing carcinoma showing well organized actin (red) morphology. *B,* A 2%

POH-treated, regressing carcinoma showing accumulated actin aggregates (red, arrow heads) relative to the well organized actin morphology of control carcinomas. *C,* A 2% POH-treated, non-regressing carcinoma showing well organized actin morphology. *D,* Control, non-regressing carcinoma showing autolysed actin from a necrotic region of the tumor. Actin was stained with BODIPY 581/591 phallacidin and nuclei were counterstained with Hoechst 33342. (*A-D*) Tissue sections visualized by epifluorescence microscopy. *E,* 2% POH-treated, regressing carcinoma showing initial intracellular actin aggregate (boxed area) formation in one of the two apoptotic cells (solid arrows) shortly before being sloughed off into a lumen-like structure . *F,* Enlargement of boxed area in (*E*). *G-H,* 2% POH-treated, regressing carcinomas showing early (*G*) and late (*H*) stages of extracellular actin aggregate accumulation in lumen-like structures. (*E-H*) Tissue sections visualized by electron microscopy.

FIG. 5. **Formation of Actin Aggregates During the Involution Stage of Mammary Gland Differentiation.** *A,* Virgin *B,* pregnant *C,* lactation *D,* and involution stages of mammary gland differentiation stained for actin (red) and nuclei (blue). The virgin, pregnant and lactation stages of mammary gland differentiation exhibit well organized actin morphology while the involution stage of differentiation shows formation of actin aggregates (arrow heads). Actin was stained with BODIPY 581/591 phallacidin and nuclei were counterstained with Hoechst 33342. Tissue sections visualized by epifluorescence microscopy.

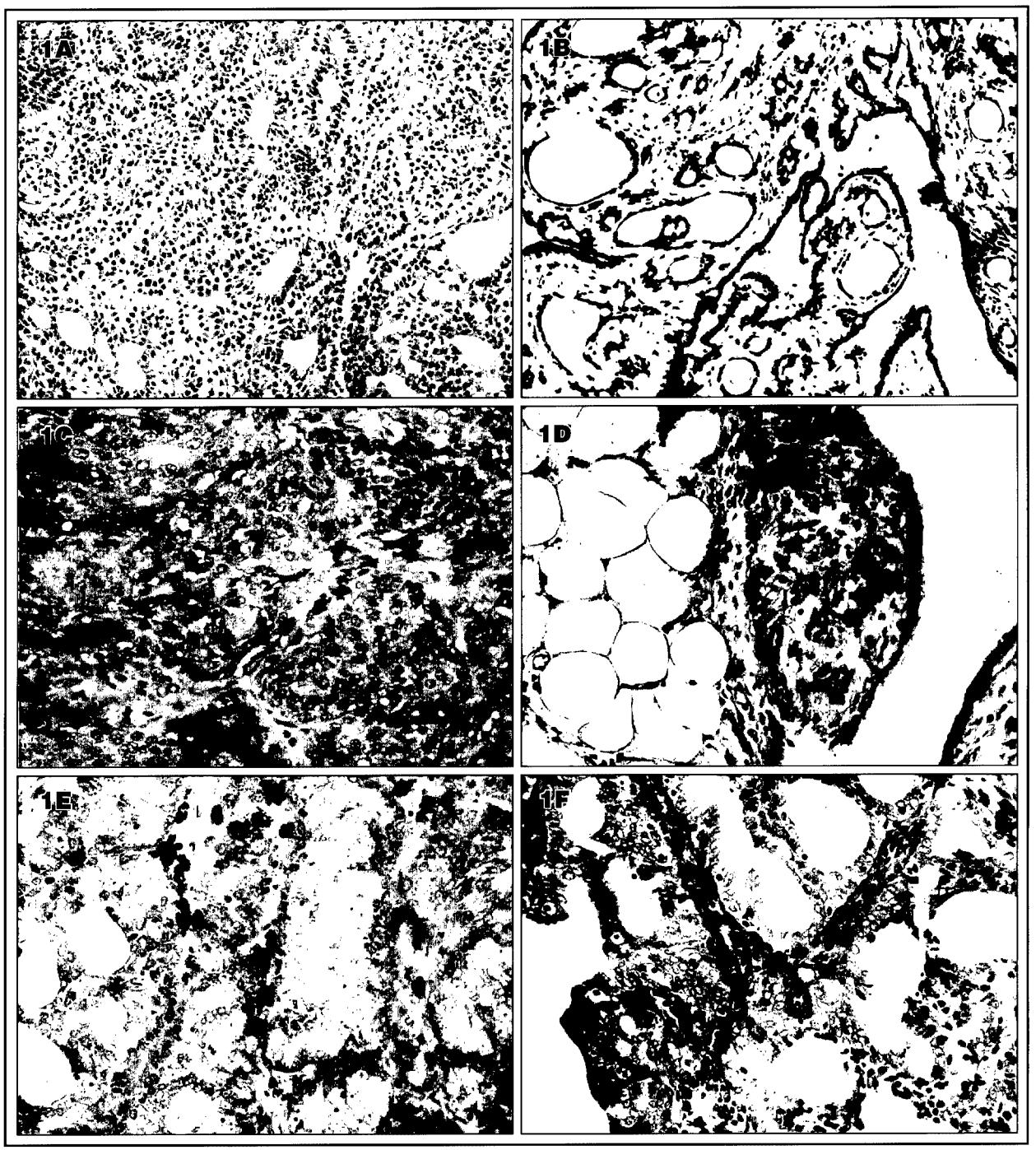

Figure 1

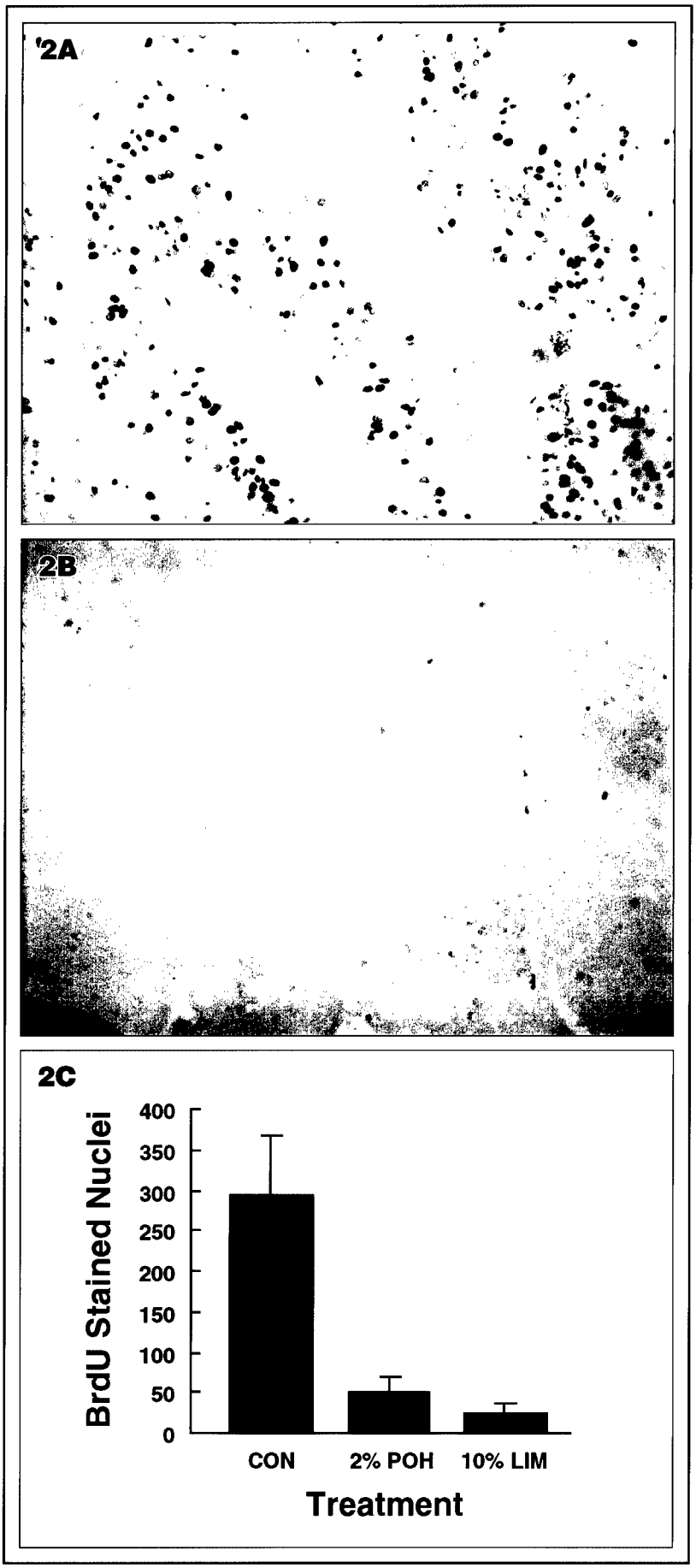
2A
2B
2C
BrdU Stained Nuclei
400
350
300
250
200
150
100
50
0
CON
2% POH
10% LIM
Treatment

Figure 2

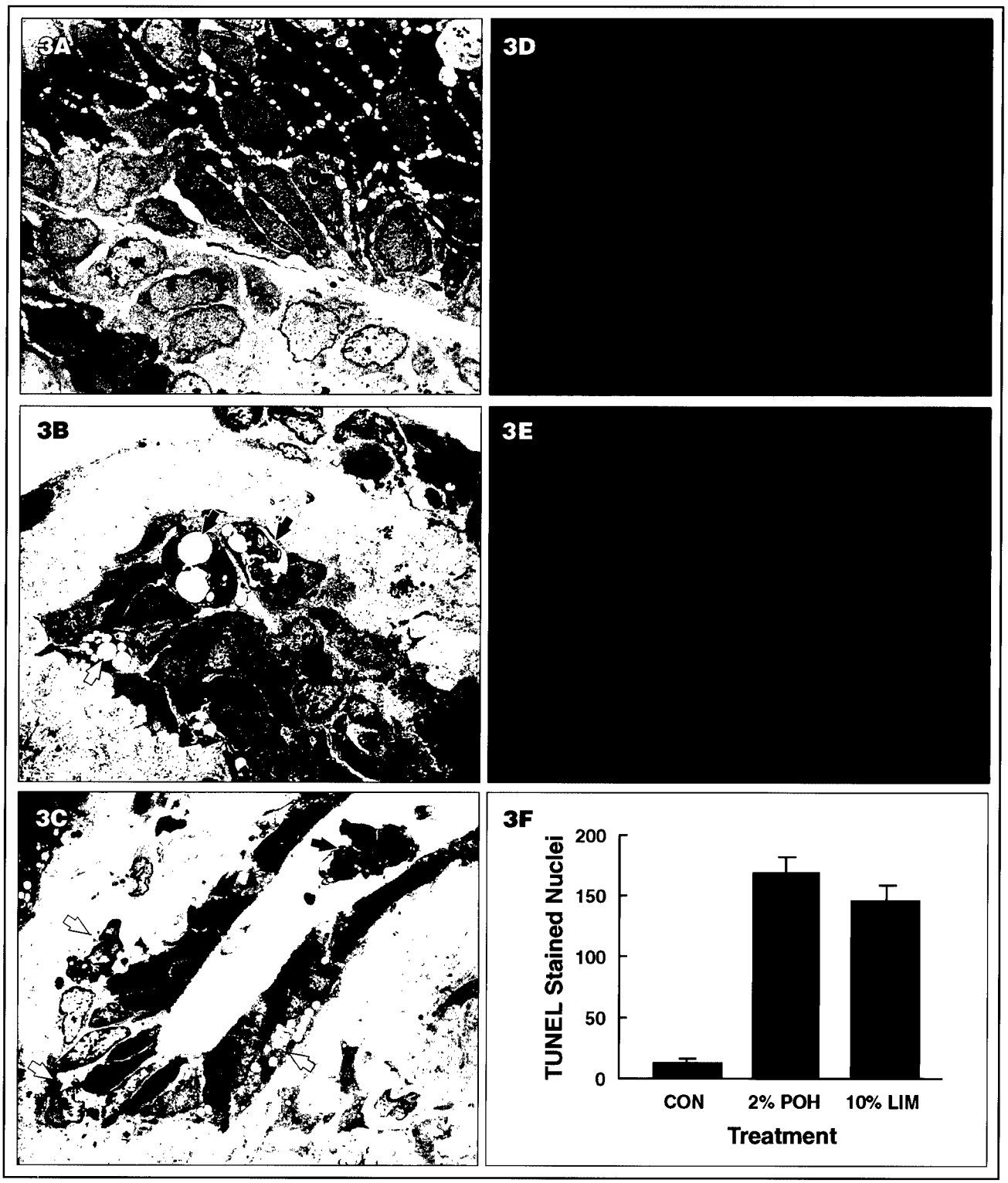
3A
3D
3B
3E
3C
3F
TUNEL Stained Nuclei
200
150
100
50
0
CON
2% POH
10% LIM
Treatment

Figure 3

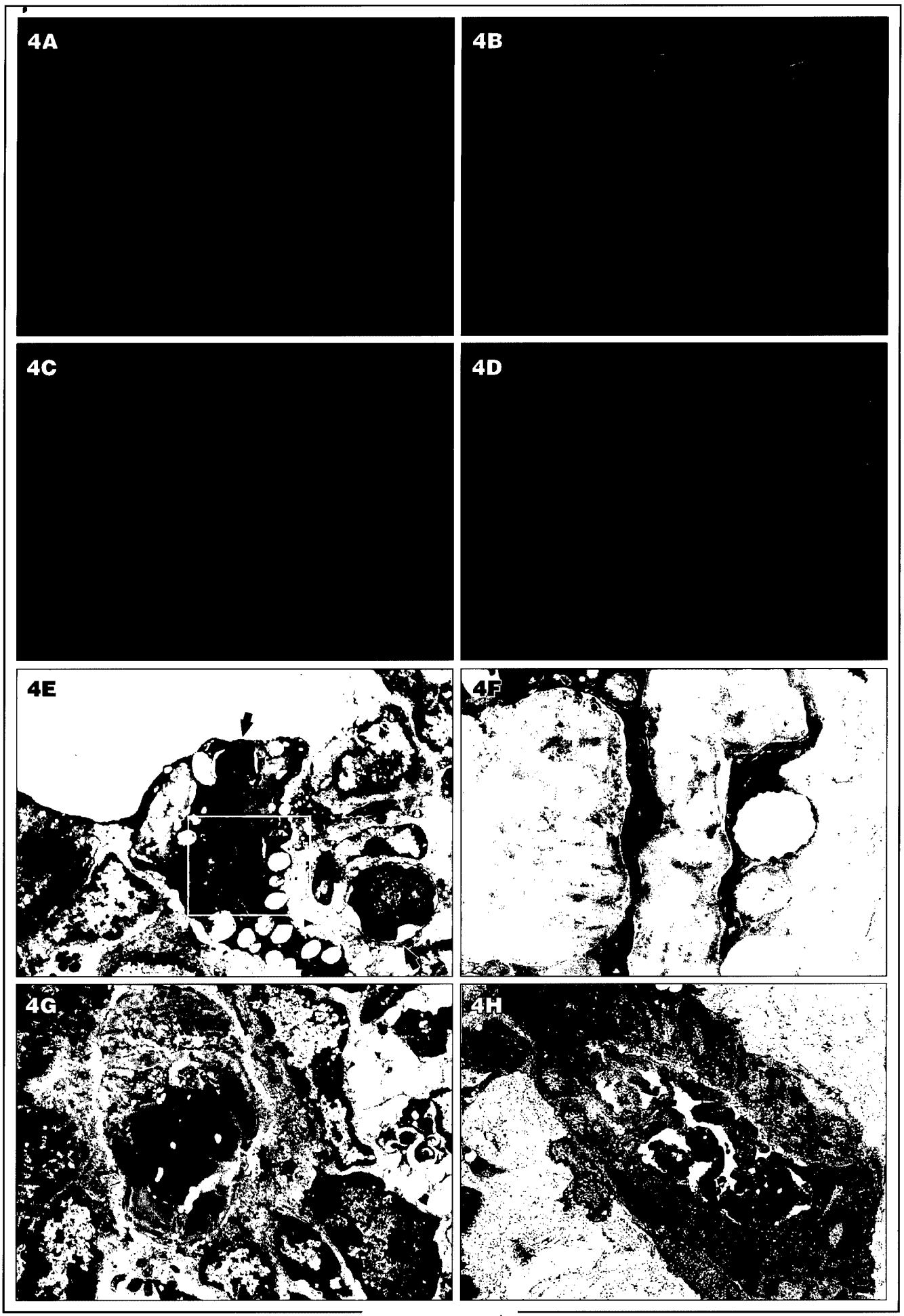

Figure 4

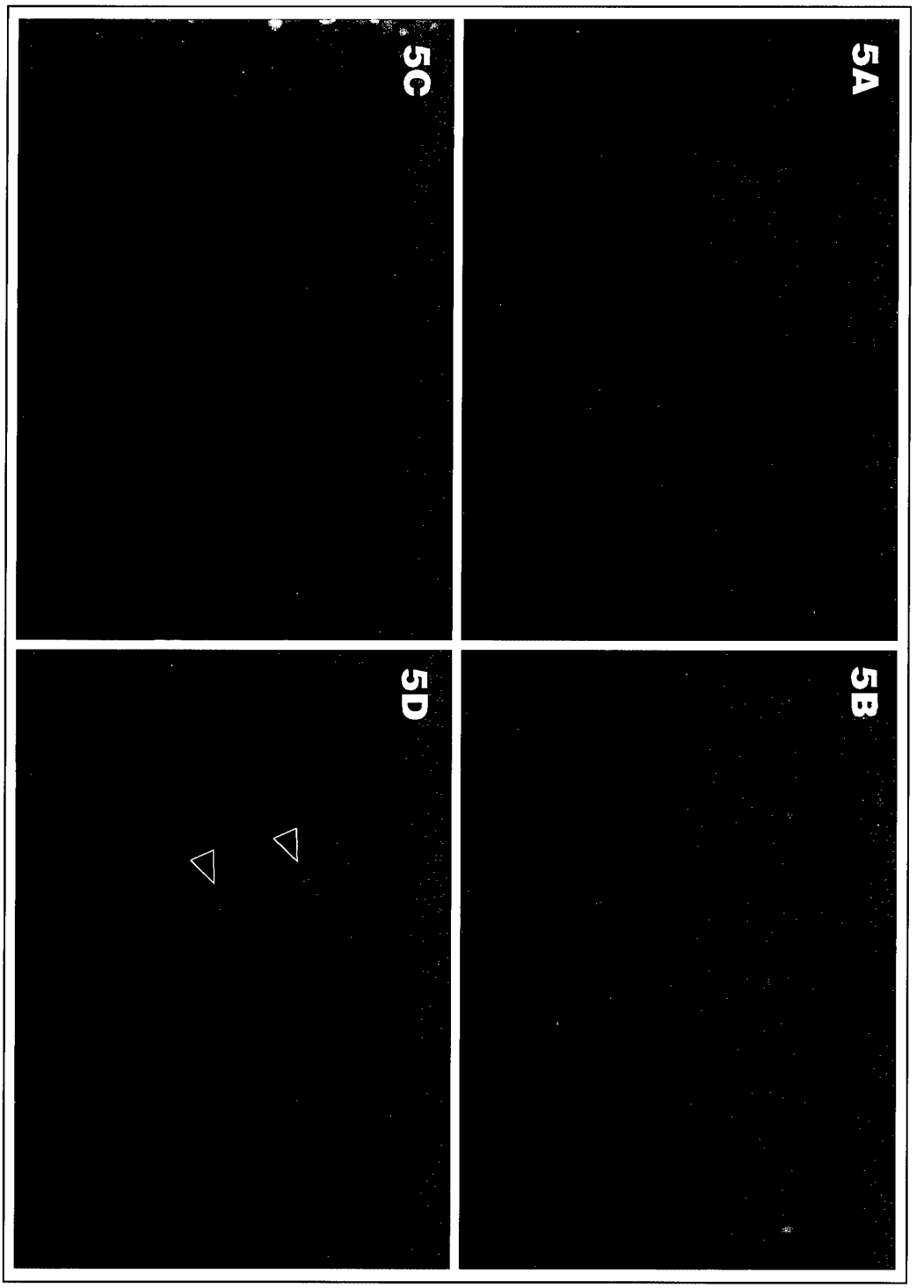

Figure 5